1101-1107
34. Cormack, B. P., Valdivia, R. H. and Falkow, S. (1996) Gene. **173**, 33-38
35. Yang, T. T., Cheng, L. and Kain, S. R. (1996) Nucleic Acids Res. **24**, 4592-4593
36. Bercovich, Z., Rosenberg-Hasson, Y., Ciechanover, A. and Kahana, C. (1989) J Biol Chem. **264**, 15949-15952
37. Cheng, Z., Garvin, D., Paguio, A., Stecha, P., Wood, K., Fan, F. (2010) Curr Chem Genomics. 4, 84-91
38. Morrison, T. B., Weis, J. J., Wittwer, C. T. (1998) Biotechniques **24**, 960-962
39. Hershko, A. and Ciechanover, A. (1998) Annu Rev Biochem. **67**, 425-479

Figure legends

Figure 1 Detection of heterogeneity of Nef expression levels. HEK293 cells transiently expressing each Nef using the pcDNA3.1 vector (A) or two clones of HEK293/CD4 cells expressing Nef_{NL4-3} or Nef_{JR-CSF} using the pcDNA4/HisMAX vector (B) were lysed and subjected to 5-20% SDS-PAGE, followed by western blot analysis using anti-V5 and anti-actin antibodies as described in Materials and Methods. The basic characteristics of the vector used in A and B are depicted in the bottom of the figure. The vector used in B has a translational enhancer sequence SP163 at upstream of the Nef coding region.

Figure 2 Immunostaining of Nef_{NL4-3} and Nef_{JR-CSF} expressed in HEK293/CD4 cells. The HEK293/CD4/Nef_{NL4-3} (top row) and HEK293/CD4/Nef_{JR-CSF} (bottom row) cells, which are stable Nef-expressing clonal cell lines, were immunostained using an anti-V5 antibody and an anti-mouse-FITC secondary antibody for Nef detection. The nucleus was stained with DAPI. The cells were observed using a Biozero digital microscope. Scale bar = 50 μm (rightmost panels).

Figure 3 Comparison of CD4 downregulation activities between Nef_{NL4-3} and Nef_{JR-CSF}. HEK293/CD4/Nef_{NL4-3} (top row panels) and HEK293/CD4/Nef_{JR-CSF} (bottom row panels) cells, which are stable Nef-expressing clonal cell lines, were stained with a PE-conjugated anti-CD4 antibody and then analyzed using a flow cytometer. HEK293/CD4 cells are depicted with the gray filled histogram, Nef-expressing HEK293/CD4 cells are depicted by the solid black line, and HEK293 cells are depicted in the striped histogram. Each MFI value is of the CD4 level in the cells expressing each Nef.

Figure 4 Induction of low expression property by AA129-206 of Nef_{NL4-3}

HEK293 cells were transiently transfected with each Nef, EGFP, or the Rluc fusion protein expression plasmid. The expression level of each Nef after 48-h transfection was analyzed by western blot analysis using an anti-V5 (B) or anti-Xpress antibody (D and E), as described in Materials and Methods. (A) Schematic representations of Nef_{NL4-3}, Nef_{JR-CSF}, and chimera Nef tested in "B". "B" shows a comparison of Nef_{NL4-3}, Nef_{JR-CSF}, and chimera Nef. (C) Schematic representations of EGFP, EGFP-NLAA129-206, and EGFP-CP tested in "D", EGFP, NLAA129-206-EGFP, and CP-EGFP tested in "E", and Rluc, NLAA129-206-Rluc, and CP-Rluc tested in "F". "D" shows a comparison of EGFP and AA129-206 or CP fusion to the *C*-terminal end of EGFP. "E" shows a comparison of EGFP and AA129-206 or CP fusion to the *N*-terminal end of EGFP. An asterisk marks an EGFP modified with unidentified posttranslational modification. "F" shows a comparison of Rluc and AA129-206 or CP fusion to the *N*-terminal end of Rluc. Rluc level was evaluated by measuring bioluminescent activity using coelenterazine h as the substrate, as described in Materials and Methods. Each bar represents the mean standard deviation (n = 3).

Figure 5 Comparison of low expression property of each deletion mutant.

(A) Schematic representations of NLAA129-206-EGFP or Rluc, NLAA142-206-EGFP or Rluc, NLAA129-186-EGFP or Rluc, and NLAA142-186-EGFP or Rluc tested in "A" or "B". HEK293 cells were transiently transfected with each EGFP or the Rluc fusion protein expression plasmid. The expression level of each fusion protein after 48-h transfection was analyzed by western blot analysis using an anti-Xpress antibody (B) or by measuring the bioluminescent activity of Rluc using coelenterazine h as the substrate (C) as described in Materials and Methods. Each bar represents the mean standard deviation (n = 3). Asterisks mark EGFPs modified with unidentified posttranslational modification (B).

Figure 6 Induction of low expression property by *C*-terminal region of Nef_{mac239} and Nef_{JR-CSF}.

(A) Schematic representations of EGFP or Rluc, CP-EGFP or CP-Rluc, macAA161-263-EGFP or macAA161-263-Rluc, and JRAA139-216-EGFP or JRAA139-216-Rluc tested in "B" or "C". HEK293 cells were transiently transfected with each expression plasmid of EGFP or Rluc and the CP, macAA161-263, and

JRAA139-216 fusion to the *N*-terminal end of EGFP or Rluc. The expression level of each fusion protein after 48-h transfection was analyzed by western blot analysis using an anti-Xpress antibody (B) or by measuring the bioluminescent activity of Rluc using coelenterazine h as the substrate (C), as described in Materials and Methods. Each bar represents the mean standard deviation (n = 3).

Figure 7 Quantification of mRNA levels by RT-qPCR
HEK293 cells were transfected with the Nef_{NL4-3}, Nef_{JR-CSF}, AA129-206-EGFP, CP-EGFP, or EGFP expression plasmid. Total RNA was extracted from these HEK293 cells and subjected to reverse transcription reaction, followed by qPCR using the Syber Green method. mRNA level was normalized to the transcript of the neomycin resistance gene, which is coded in the expression vector used. Each bar represents the mean standard deviation (n = 3). (A) Comparison of mRNA level between Nef_{NL4-3} and Nef_{JR-CSF}. (B) Comparison of mRNA level among AA129-206-EGFP, CP-EGFP, and EGFP

Figure 8 Effect of proteasome inhibitor on expression levels of Nef_{NL4-3} and AA129-206-EGFP
HEK293 cells expressing Nef_{NL4-3} (A) or AA129-206-EGFP (B) were treated with 20 μM MG132 for 0, 3, and 6 h. The expression levels of Nef_{NL4-3} and AA129-206-EGFP in HEK293 cells were analyzed by western blot analysis. The intensities of the bands were semiquantified with Fujifilm Image Gauge Software. The intensities of Nef_{NL4-3} and AA129-206-EGFP were normalized to that of actin. Each bar represents the mean standard deviation (n = 3).

Figure 1

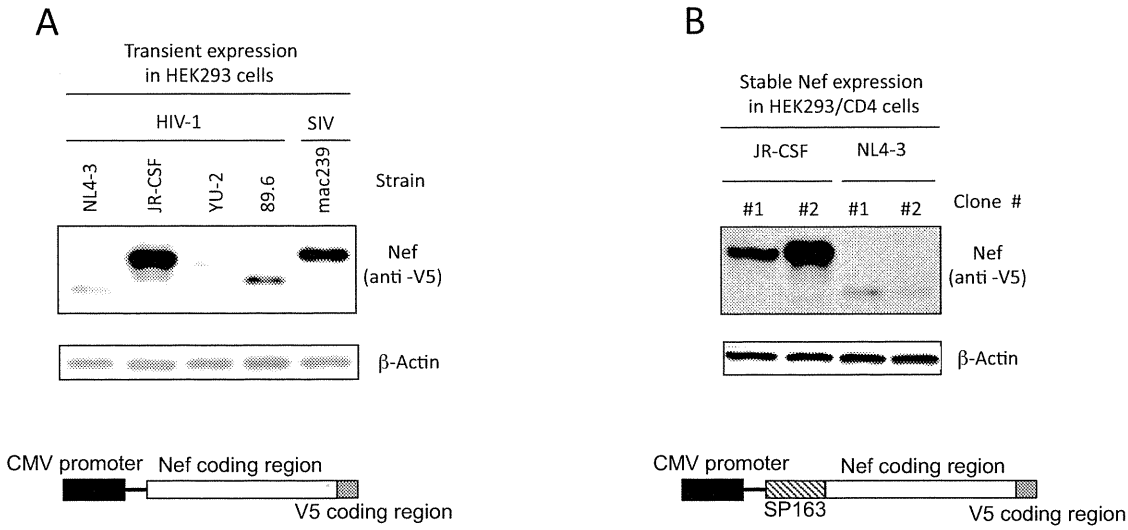

Figure 2

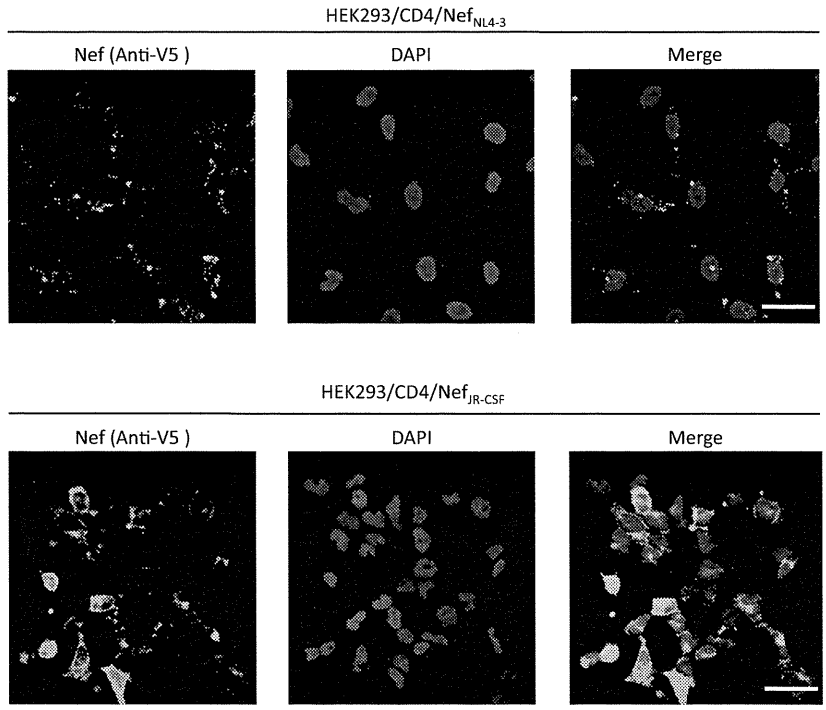

Figure 3

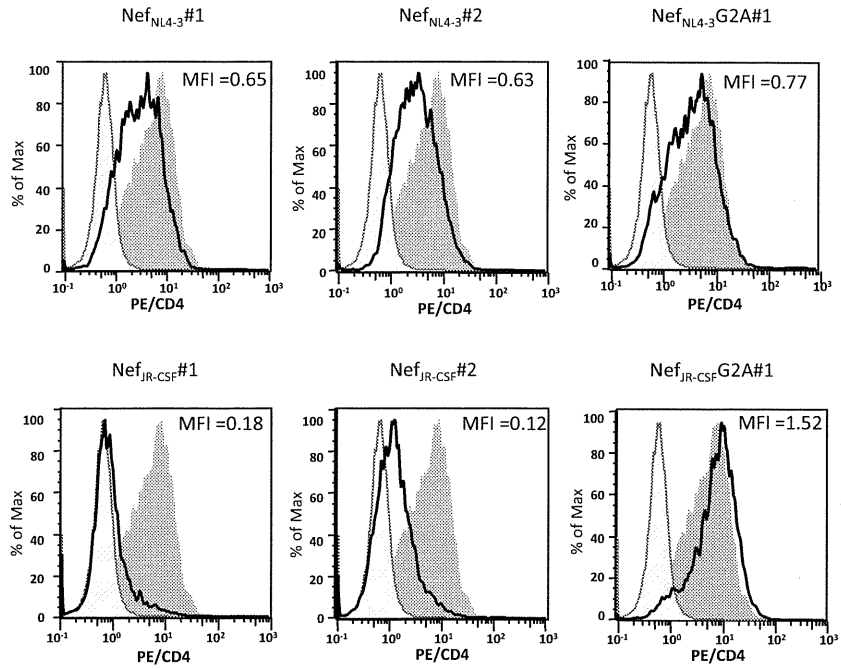

Figure 4

A

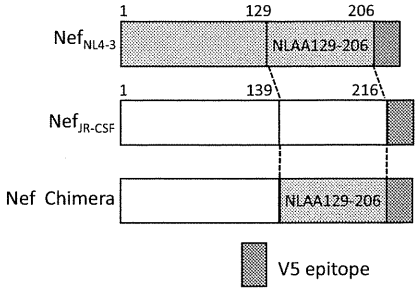

B

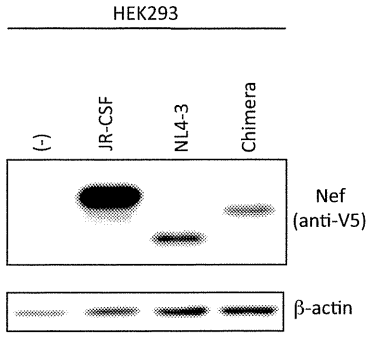

C

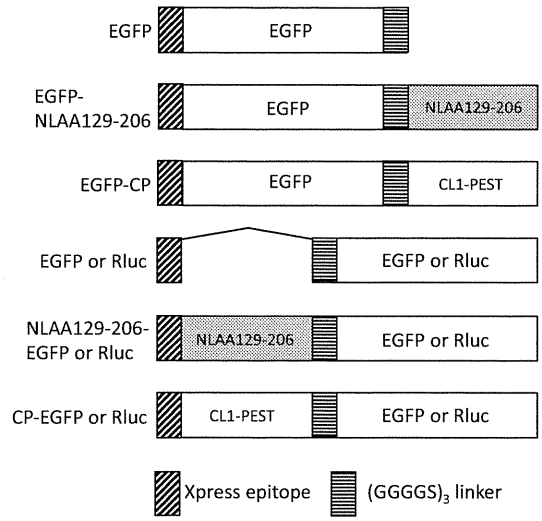

Figure 4

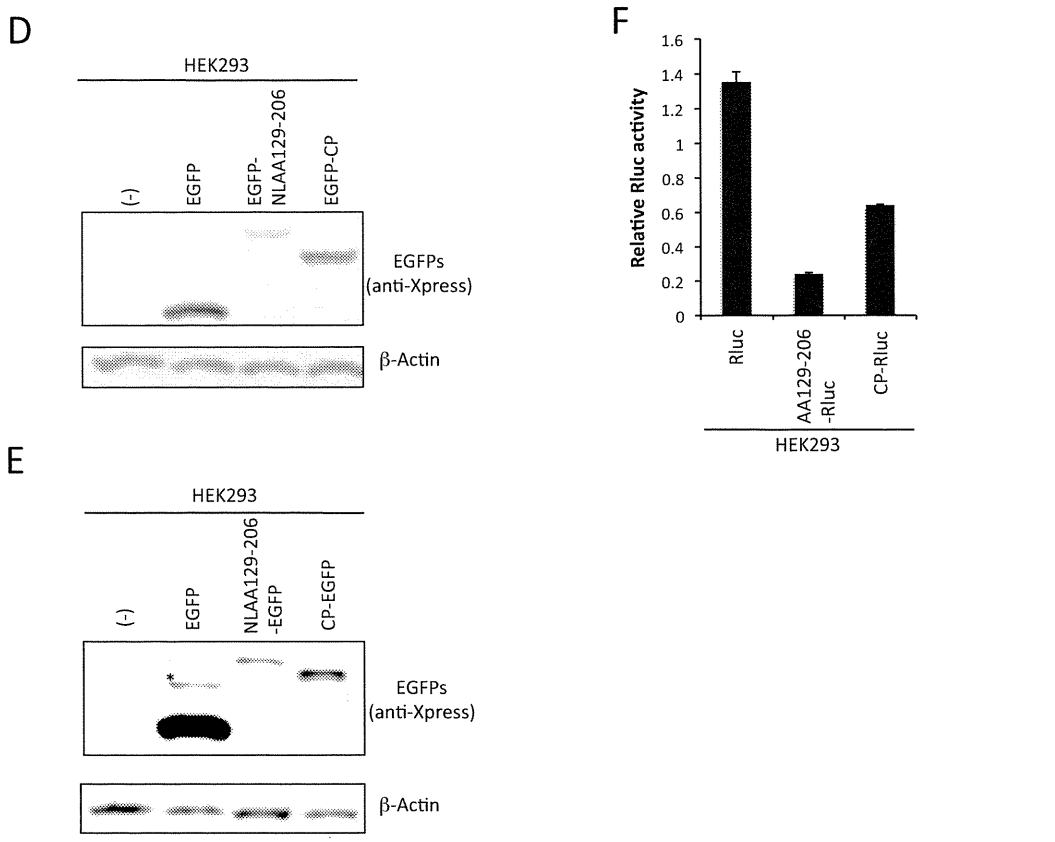

Figure 5

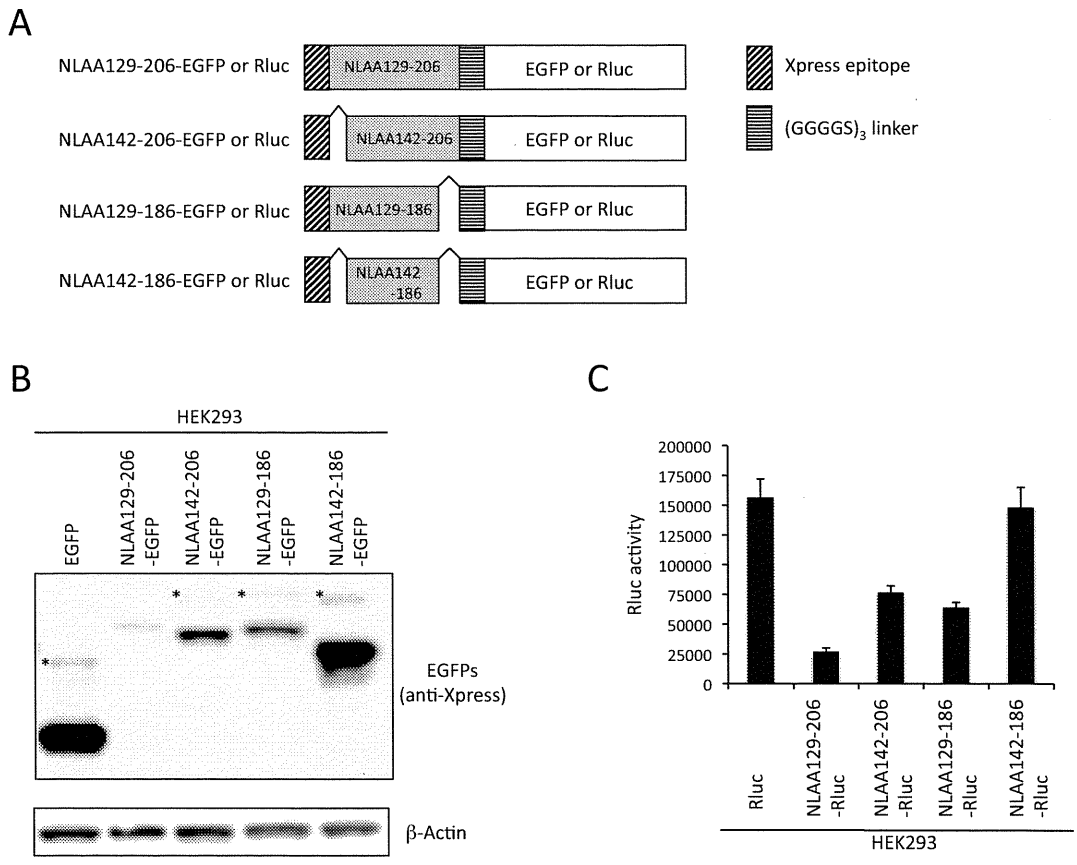

Figure 6

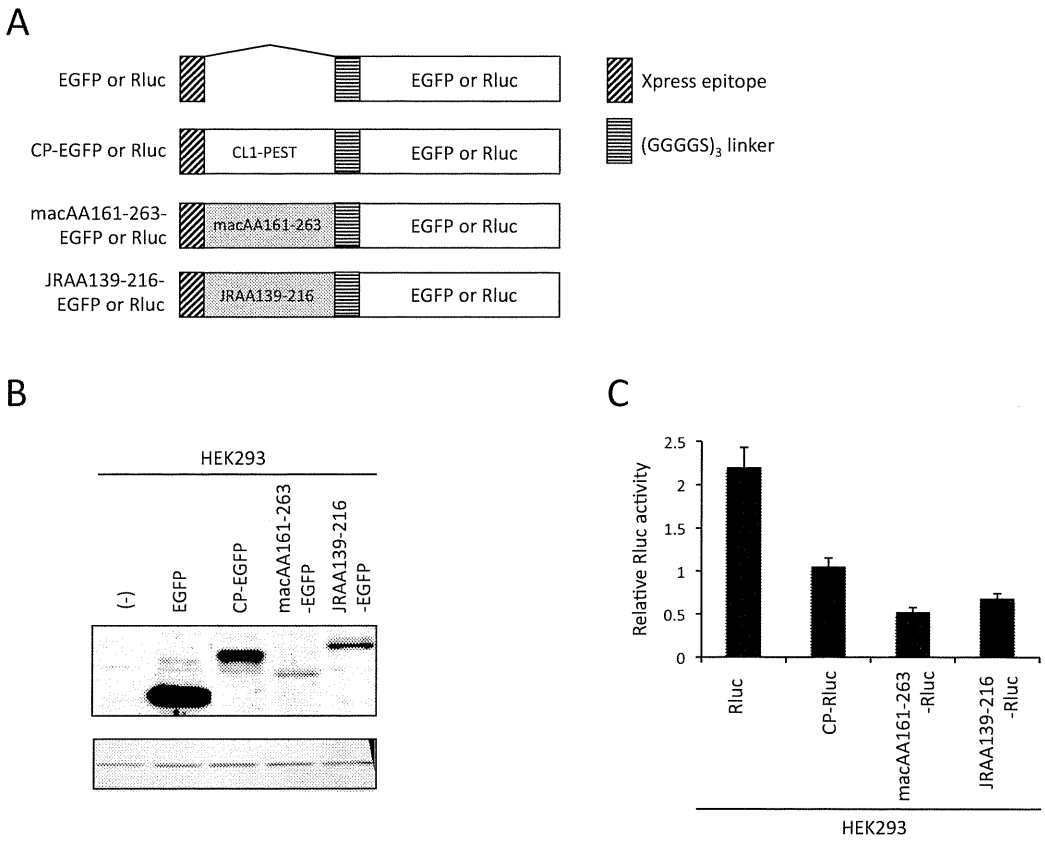

Figure 7

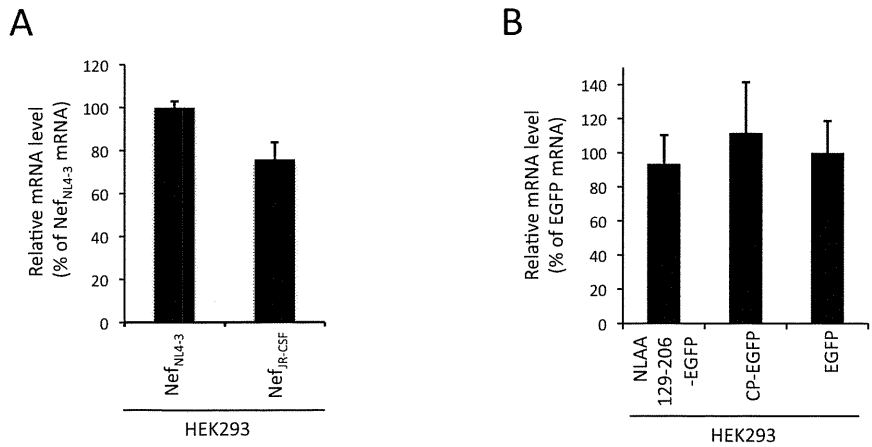

Figure 8

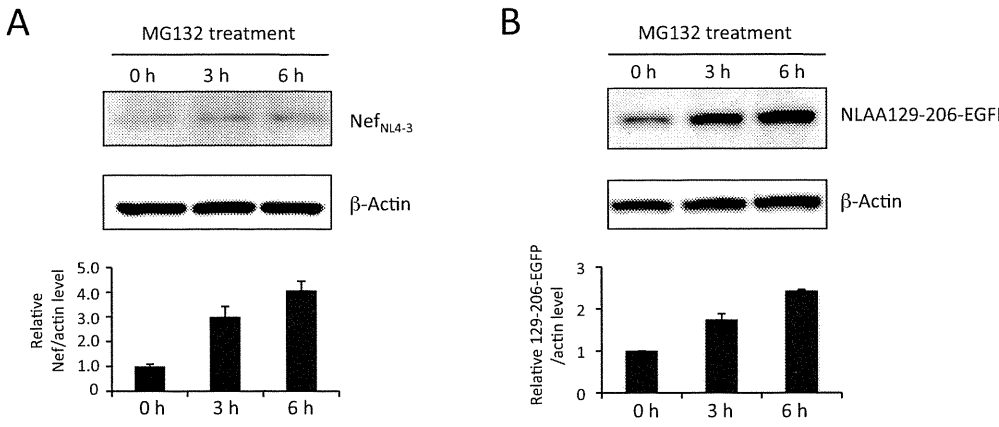
A
MG132 treatment
0 h
3 h
6 h
Nef$_{NL4-3}$
β-Actin
Relative Nef/actin level
5.0
4.0
3.0
2.0
1.0
0
0 h
3 h
6 h
B
MG132 treatment
0 h
3 h
6 h
NLAA129-206-EGFP
β-Actin
Relative 129-206-EGFP /actin level
3
2
1
0
0 h
3 h
6 h

BIOCHEMISTRY
including biophysical chemistry & molecular biology

Article

pubs.acs.org/biochemistry

Effects of DNA Binding of the Zinc Finger and Linkers for Domain Fusion on the Catalytic Activity of Sequence-Specific Chimeric Recombinases Determined by a Facile Fluorescent System

Wataru Nomura,*[,†] Akemi Masuda,[†,‡] Kenji Ohba,[§] Arisa Urabe,[†] Nobutoshi Ito,[‡] Akihide Ryo,[∥] Naoki Yamamoto,[§] and Hirokazu Tamamura*[,†,‡]

[†]Institute of Biomaterials and Bioengineering, Tokyo Medical and Dental University, 2-3-10 Kandasurugadai, Chiyoda-ku, Tokyo 101-0062, Japan

[‡]Graduate School of Biomedical Science, Tokyo Medical and Dental University, 1-45 Yushima, Bunkyo-ku, Tokyo 113-8510, Japan

[§]Department of Microbiology, Yong Loo Lin School of Medicine, National University of Singapore, Singapore 117597, Singapore

[∥]Department of Microbiology and Molecular Biodefense Research, School of Medicine, Yokohama City University, 3-9 Fukuura, Kanazawa-ku, Yokohama 236-0004, Japan

S *Supporting Information*

ABSTRACT: Artificial zinc finger proteins (ZFPs) consist of Cys_2-His_2-type modules composed of ~30 amino acids with a $\beta\beta\alpha$ structure that coordinates a zinc ion. ZFPs that recognize specific DNA target sequences can substitute for the binding domains of enzymes that act on DNA to create designer enzymes with programmable sequence specificity. The most studied of these engineered enzymes are zinc finger nucleases (ZFNs). ZFNs have been widely used to model organisms and are currently in human clinical trials with an aim of therapeutic gene editing. Difficulties with ZFNs arise from unpredictable mutations caused by nonhomologous end joining and off-target DNA cleavage and mutagenesis. A more recent strategy that aims to address the shortcomings of ZFNs involves zinc finger recombinases (ZFRs). A thorough understanding of ZFRs and methods for their modification promises powerful new tools for gene manipulation in model organisms as well as in gene therapy. In an effort to design efficient and specific ZFRs, the effects of the DNA binding affinity of the zinc finger domains and the linker sequence between ZFPs and recombinase catalytic domains have been assessed. A plasmid system containing ZFR target sites was constructed for evaluation of catalytic activities of ZFRs with variable linker lengths and numbers of zinc finger modules. Recombination efficiencies were evaluated by restriction enzyme analysis of isolated plasmids after reaction in *Escherichia coli* and changes in EGFP fluorescence in mammalian cells. The results provide information relevant to the design of ZFRs that will be useful for sequence-specific genome modification.

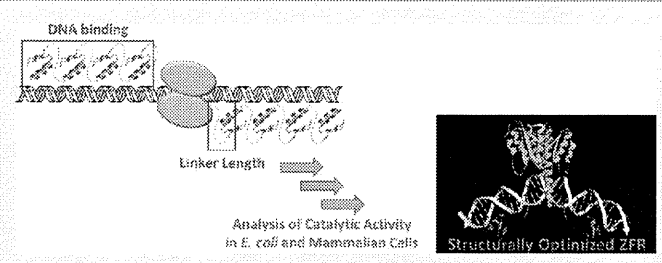

Artificial zinc finger proteins (ZFPs) can be used to engineer DNA binding domains with high specificity for desired target sequences, and ZFPs are a promising technology for gene therapy.[1−6] Modular assembly of ZFPs can create a DNA binding domain that targets virtually any sequence in the human genome.[3−5] By linking ZFPs to the catalytic domains of DNA-modifying enzymes, novel enzymes, including nucleases,[6] recombinases,[7−12] and methylases,[13−20] have been fabricated. These enzymes are endowed with programmable DNA binding specificity provided by the zinc finger protein fusion. Relevant to our development of ZFRs, recombinase enzymes from the serine recombinase family have been well studied.[21] In comparison with members of the tyrosine recombinase family such as Cre and Flp recombinases, the serine recombinases, including Tn3 and $\gamma\delta$ resolvases, Hin invertase, and Gin invertase, have DNA binding domains that are structurally independent of the catalytic domain. The structures of the catalytic domains and the sequences required for catalytic activity are highly conserved in these recombinases.[22] Tn3 and $\gamma\delta$ are among the best-characterized site-specific recombinase enzymes in the serine recombinase family. Only 35 amino acid residues differ between the $\gamma\delta$ and Tn3 resolvases, and their structures and functions are similar.[23] Negatively supercoiled DNA is a prerequisite for substrate recombination with native serine recombinase enzymes.[21] Although it is known that native serine recombinases require accessory proteins binding to sites I−III, activating mutants that require only the 28 bp of site I for successful recombination have been isolated.[7] In these hyperactivated enzymes, a DNA substrate in the form of negatively supercoiled DNA is not required for activity, and this allows application of activated catalytic domains with ZFPs to create zinc finger recombinases (ZFR). It has been suggested that reactions with serine recombinases proceed in three

Received: December 19, 2011
Revised: January 21, 2012

steps: (i) formation of a dimer binding to the two forms of site I on the DNA, (ii) formation of a tetramer between the forms of site I, and (iii) strand exchange.[24,25] After the strand exchange reaction, the sequences between target sites are excised and the strands ligated (Figure 1).

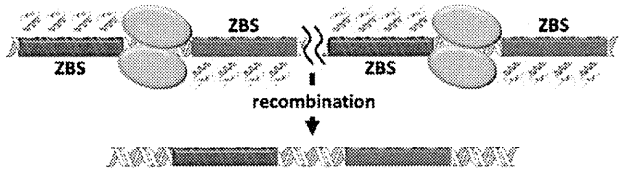

Figure 1. Schematic illustration of the ZFR reaction at a target site. The green and red boxes represent zinc finger binding sites (ZBSs). The yellow spheres represent catalytic domains of Tn3 resolvase.

ZFRs based on catalytic domain variants of Tn3, Gin, and Hin fused to artificial ZFPs have been shown to catalyze site-specific recombination in *Escherichia coli*[7−11] and mammalian cells.[8,9,11,12] ZFRs have also been shown to catalyze high-fidelity site-specific integration in mammalian cells.[9,11,12] While directed evolution of recombinase catalytic domains has proven to be essential for developing ZFR enzymes that function in mammalian cells, other aspects of ZFR design have not been thoroughly studied. In this report, we have synthesized ZFR mutants with variable numbers of zinc fingers and studied the role of peptide linkers that connect the Tn3 resolvase catalytic domain with the ZFP DNA binding domain. These effects are not readily addressed using molecular evolution strategies. For facile evaluation of recombination reactions in mammalian cells, a system that allows evaluation within 48 h was developed utilizing DsRed expression as a marker of transfection efficiency and EGFP expression as a marker of recombination efficiency. The results obtained revealed the optimal structures of the ZFRs, and the recombination efficiency results for linker mutants were verified by modeling studies.

EXPERIMENTAL PROCEDURES

Construction of ZFP Genes. ZFP genes were constructed as described previously.[26,27] Briefly, plasmid pc3XB encoding ZFPs purchased from Addgene (http://www.addgene.org) was repeatedly ligated. The zinc finger gene that was obtained was inserted into pMAL-p4x as an *Xba*I−*Bam*HI fragment for protein expression. A minor change was made to the multiple cloning site of pMAL-p4x (Figure S1 of the Supporting Information).

Target Enzyme-Linked Immunosorbent Assays (ELISAs). ELISA wells of 96-well plates were coated by incubation with 25 μL of 8 ng/mL streptavidin in PBS for 1 h at 37 °C. The plates were washed twice with dH_2O, and 25 μL of 5′-biotinylated hairpin oligonucleotide target in zinc buffer A (ZBA) [10 mM Tris-HCl (pH 7.5), 90 mM KCl, 1 mM $MgCl_2$, and 90 μM $ZnCl_2$] was added. After incubation for 1 h at 37 °C, plates were washed twice with dH_2O. Blocking solution (ZBA with 3% BSA, 175 μL) was added, and incubation continued for 1 h at 37 °C. The blocking solution was then removed; 25 μL of purified protein in ZBA was added, and 2-fold serial dilutions were performed into 1% BSA, 5 mM DTT, and 10 ng/μL salmon sperm DNA in ZBA. After incubation for 1 h at room temperature, the plates were washed 10 times with dH_2O and the monoclonal anti-MBP antibody (Sigma-Aldrich, 1:1000 dilution by ZBA with 1% BSA, 25 μL) was added. After incubation for 30 min at room temperature, the plates were washed 10 times with dH_2O and a diluted secondary anti-mouse IgG AP conjugate (Sigma-Aldrich, 1:1000 dilution by ZBA with 1% BSA, 25 μL) was added. After incubation for 30 min at room temperature, plates were washed 10 times with dH_2O. The alkaline phosphatase reaction was performed with *p*-nitrophenylphosphate for 30 min, and the absorbance at 405 nm was read with a microplate reader. The data were collected and plotted. The data were fit to the equation $y = 1/(1 + K_d/x)$, where y is the proportion of bound MBP−ZFP fusion protein to maximal binding derived from the absorbance at 405 nm and x is the concentration of the MBP−ZFP fusion protein. The K_d values are averages of three or more independent experiments, and standard errors of the mean (SEM) are shown.

Construction of ZFR Substrates. Each substrate plasmid contained a recombination cassette composed of two ZFR recombination sites flanking an EGFP gene as a stuffer sequence. Cassettes were assembled by amplifying the EGFP gene with primers encoding the ZFR site. The polymerase chain reaction (PCR) product was cloned into pAra-OP.[20] ZFP genes were amplified by PCR from plasmid pc3XB and inserted into the plasmid as *Eco*RI−*Sac*I fragments. Plasmids that contained ZFR with Gly-Ser linkers were mutated at the *Bst*BI site before insertion of the catalytic domain.

Construction of ZFR Genes. The DNA fragment of the Tn3 resolvase catalytic domain was amplified from pWL625 (ATCC accession number 31787) utilizing 5′-GAGGAGGAATTCATGCGACTTTTTGGTTACGCT-3′ and 5′-GAGGAGAAGCTTTCACGAGGCCCTTTCGTCTT-3′ as primers. The fragment was inserted into pBluescriptSK(−) as an *Eco*RI−*Hin*dIII fragment. Tn3-activating mutations (R2A, E56K, G101S, D102Y, M103I, and Q105L) were introduced into the Tn3 encoding gene. Linker sequences were amplified via PCR with the Tn3 fragment by primers that included the linker sequence. Tn3 fragments with different linkers were digested with *Eco*RI and *Bgl*II and ligated into similarly digested pAra-OP with the EGFP and ZFR sites. Tn3 fragments with various Gly-Ser linkers were also digested with *Eco*RI and *Bst*BI and then ligated. The plasmids were maintained with chloramphenicol.

Assay of Recombination of Plasmids in *E. coli*. The plasmid with a ZFR gene downstream from the arabinose promoter and the substrate sequences were introduced into *E. coli* by electroporation. After incubation for 14 h at 37 °C on an LB-agar plate, colonies were picked up and grown for 14 h at 37 °C in LB medium. Purified plasmids were digested with *Eco*RI for 1 h at 37 °C. After electrophoresis on a 0.8% agarose gel, the fragment intensity was estimated with ImageJ (Figure S2 of the Supporting Information).

Recombination Reaction of ZFR in Mammalian Cells. The EGFP gene, flanked by recombination sites, was inserted between *Nhe*I and *Kpn*I in pcDNA5/FRT (Life Technologies). A double-stranded oligonucleotide encoding the upstream target site was inserted into the *Mlu*I site, and the other oligonucleotide for the downstream target site was inserted into *Kpn*I and *Bam*HI sites. Cotransfection of the substrate plasmid and Flp expression plasmid (pOG44, Life Technologies) allowed site-specific integration into the single FLP recombinase target (FRT) site present in the Flp-In-CHO cell line (Life Technologies). Colony-acquired hygromycin resistance was characterized by fluorescently activated cell sorting (FACS) and genomic PCR. The sequence of the target site was confirmed. Cells were maintained in Ham's F-12 containing 10% (v/v)

Table 1. DNA Binding Affinities of ZFPs

	two fingers	three fingers	four fingers	five fingers	six fingers
K_d (nM)[a]	160±20	23.6±3.6	12.8±1.1	15.4±1.4	12.9±1.4
R^2	0.90	0.87	0.94	0.94	0.94

[a]The values are averages of three or more independent experiments.

FBS and antibiotics (Wako Chemicals). The DsRed expression vector was constructed as follows; a DsRed-monomer sequence was ligated into pIRES2-EGFP (Clontech) to substitute for EGFP, and a Tn3-ZFP-NLS fragment was inserted between *Nhe*I and *Eco*RI in pIRES2-DsRed. On the following day, after 2×10^5 cells had been seeded, the ZFR expression vector was transfected into cells using Lipofectamine LTX Reagent and PLUS Reagent (Life Technologies). After being transfected for 48 h, cells were collected and analyzed by flow cytometry.

Molecular Modeling of the Linker Variants of ZFR. Computer models were generated using Discovery Studio (Accelrys Inc.). The crystal structure of the $\gamma\delta$ resolvase–DNA complex [Protein Data Bank (PDB) entry 1GDT][22] was manually mutated in the protein and DNA to match the molecules used in this study. The first zinc finger module, obtained from a zinc finger–DNA complex (PDB entry 1MEY),[28] was placed on the resolvase–DNA complex by superimposing the phosphate backbone atoms of corresponding DNA residues. Appropriate linker atoms were then added and optimized by simulated annealing and energy minimization. During this optimization, the atoms in the resolvase, zinc fingers, and DNA were fixed, allowing only linker atoms to move.

RESULTS

Construction of Zinc Fingers and DNA Binding Analyses. The 18 bp target sequence of the zinc finger protein utilized in this study was 5′-CTGCATGCACTGGATGCA-3′.

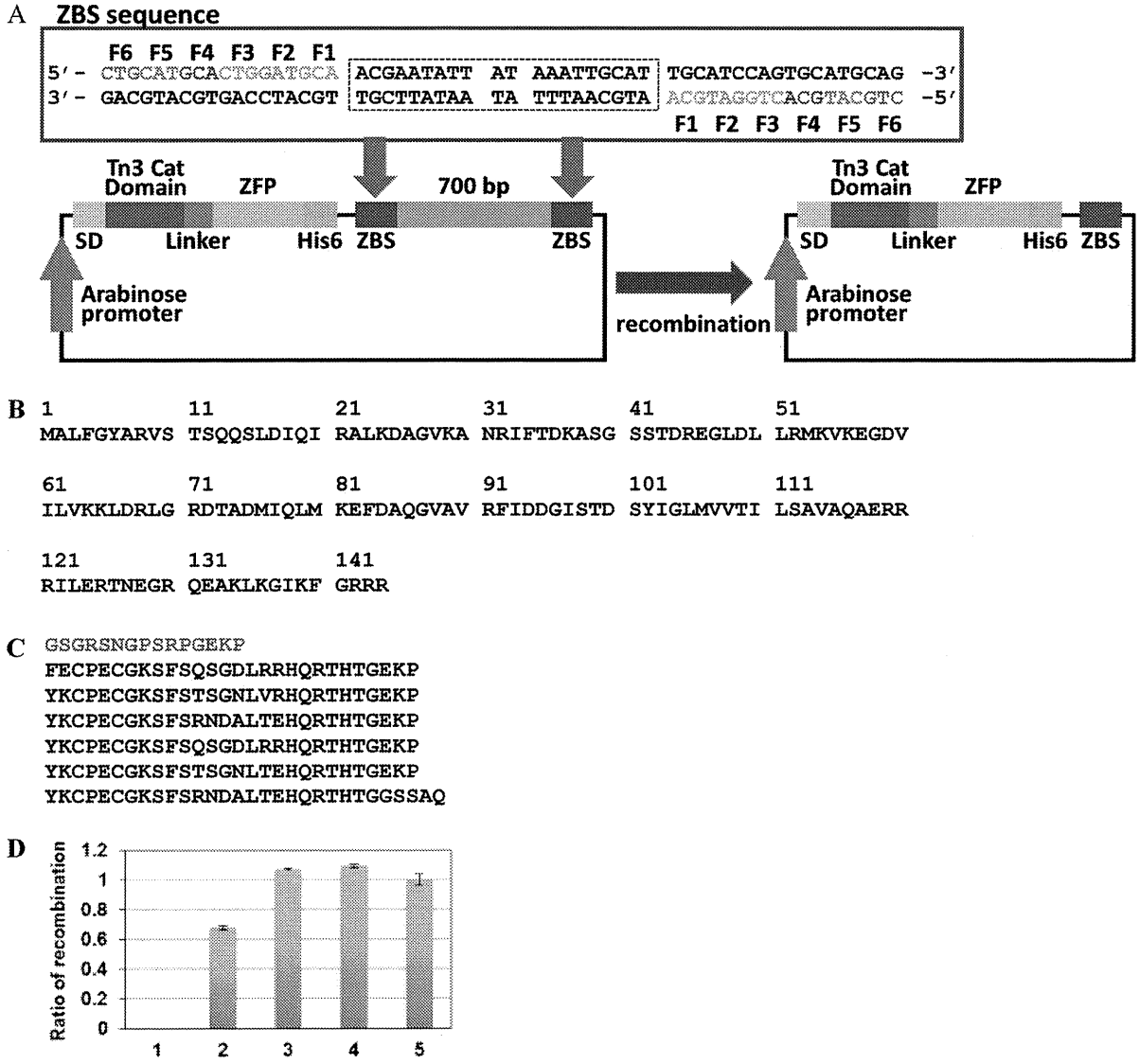

Figure 2. (A) Schematic of recombination at zinc finger binding sites (ZBSs). Recombination results in smaller plasmids. ZBS sequences are shown in the box. SD represents the Shine-Dalgarno sequence. (B) Amino acid sequences of the hyperactivated Tn3 catalytic domain. (C) Amino acid sequences of the linker (red) and six-zinc finger domain utilized for the analysis in *E. coli*. (D) Recombination efficiency depends on the number of fingers in ZFR. Columns 1–5 show the recombination efficiencies of two- through six-finger modules. The ratios are relative to the efficiency of the six-finger module. The error bars show the SEM of three or more independent experimental results.

A

```
Clone 1.          R RSNGPSRPGEKP
Clone 2. IKF      R RSNGPSRPGEKP
Clone 3. IKF GRRR
Clone 4. IKF GRRR EKP
Clone 5. IKF GRRR RPGEKP
Clone 6. IKF GRRR GPSRPGEKP
Clone 7. IKF GRRR RSNGPSRPGEKP
Clone 8. IKF GRRR GSGRSNGPSRPGEKP
Clone 9. IKF GRRR GSGGGSRSNGPSRPGEKP
Clone 10.IKF GRRR GSGGGSGGSRSNGPSRPGEKP
Clone 11.IKF GRRR GSGGGSGGSGGSRSNGPSRPGEKP
Clone 12.IKF GRRR GSGGGSGGSGGSGGSRSNGPSRPGEKP
Clone 13.IKF GRRR GSGGGSGGSGGSGGSGGSRSNGPSRPGEKP
Clone 14.IKF GRRR GSG
Clone 15.IKF GRRR GSGGGS
Clone 16.IKF GRRR GSGGGSGGS
Clone 17.IKF GRRR GSGGGSGGSGGS
Clone 18.IKF GRRR GSGGGSGGSGGSGGS
Clone 19.IKF GRRR GSGGGSGGSGGSGGSGGS
```

B

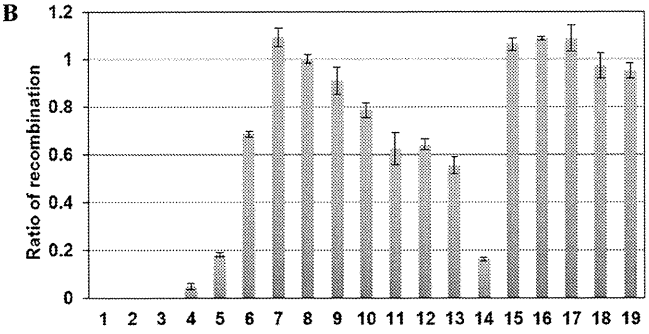

Figure 3. (A) Amino acid sequences of linkers of clones. All linkers were tested in the context of six-finger binding domains. (B) Results of recombination efficiency of clones with different linker sequences. The numbers of columns correspond to the clone numbers as described in panel A. The ratios are relative to the efficiency of clone 8. The error bars show the SEM of three or more independent experimental results.

Zinc fingers were constructed on the basis of a modular assembly strategy described by Barbas and co-workers.[27,29−32] Two- to six-finger proteins were constructed to obtain DNA binding domains with different affinities. Proteins were expressed as maltose binding protein fusions and purified with an MBPTrap column (GE Healthcare). The purity of the proteins was determined to be >90%. The DNA binding affinities were evaluated by an ELISA with the biotinylated hairpin oligonucleotide as a target.[10] The binding constants (K_d) of the two-, three-, four-, five-, and six-finger modules, listed in Table 1, were found to be 160, 23.6, 12.8, 15.4, and 12.9 nM, respectively. These results indicate that in the two-, three-, and four-finger modules, the DNA binding affinity increased with finger number but the binding affinities of ZFPs with four, five, and six fingers were similar.

Construction of ZFR Chimeric Proteins and Recombination Analysis in *E. coli*. The target DNA sequence of ZFR is shown in Figure 2A. The target site consists of a 20 bp spacer sequence flanked by 18 bp zinc finger binding sites. The spacer region was previously shown to be a Z+4 site in the target spacer of Z-resolvase.[7] For the evaluation of recombination in *E. coli*, a plasmid-based recombination system was constructed. The coding sequence of ZFRs was inserted into the plasmid containing a 700 bp stuffer sequence flanked with target sequences. In the recombination mediated by the expressed ZFRs, the stuffer sequence is excised to produce a smaller plasmid (Figure 2A). The amino acid sequences of the hyperactivated Tn3 catalytic domain, the linker between the domains, and the zinc finger domain are shown in panels B and C of Figure 2. The recombination efficiency was evaluated by a restriction enzyme assay. Plasmid purified from *E. coli* was digested by *Eco*RI, which is a single cutter of the plasmid. The linear plasmid was analyzed on an 0.8% agarose gel, and the fractions of the longer (nonrecombinant) and shorter (recombinant) plasmids were evaluated (Figure S2 of the Supporting Information). ZFR variants with different numbers of fingers were evaluated in this recombination system, and recombination ratios increased with increasing numbers of fingers from two to four fingers. The values of recombination efficiencies for ZFRs with four to six fingers were similar, reflecting the DNA binding affinities (Figure 2D). The production of recombinant sequence was confirmed by DNA sequencing analysis (Figure S3 of the Supporting Information).

In the next study, the reactions of ZFR variants with different linker lengths in the context of the six-finger module were tested (Figure 3B). In this experiment, 19 constructs were prepared. The variants were categorized into three groups depending on lengths and the compositions of linker sequences. The first group variants have short linkers with deletions within the catalytic

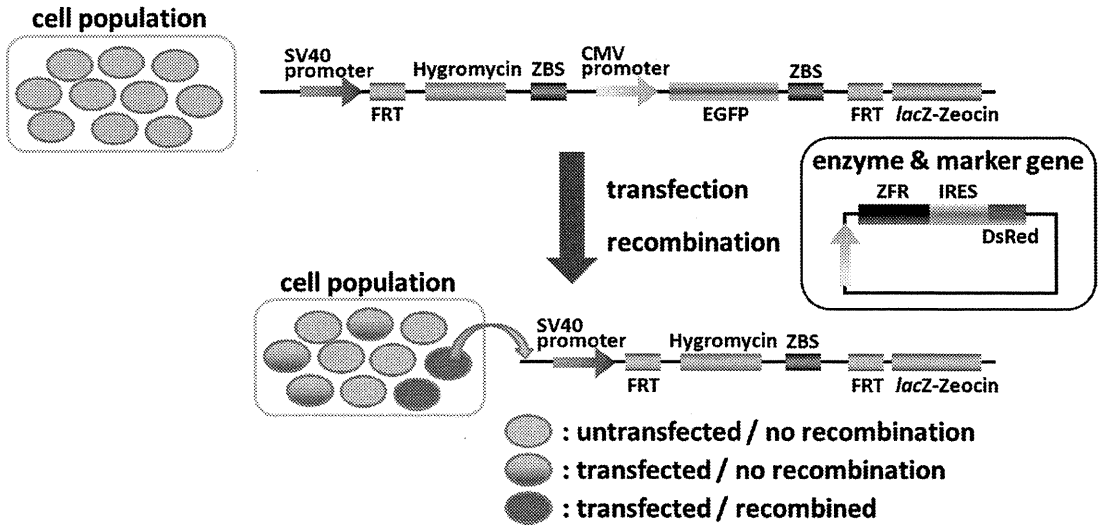

Figure 4. Recombination system constructed utilizing Flp-In-CHO-K1 cells.

dx.doi.org/10.1021/bi201878x | *Biochemistry* XXXX, XXX, XXX−XXX

domain of Tn3 resolvase (clones 1 and 2). The second group of variants has semirigid linkers (clones 3–13). The third group has flexible linker sequences composed of Gly-Ser sequences (clones 14–19). In the clones of the third group, the first two amino acids of the zinc finger domain, Tyr and Lys, are substituted with Phe and Glu, respectively. The recombination efficiencies were determined in the *E. coli*-based assay (Figure 3B). The results indicate two important phenomena. (1) The variant with a 12-amino acid linker was the most efficient (clone 7, Figure 3A), suggesting that there is an optimal linker length. (2) The variants with linkers composed of only Gly-Ser sequences were most efficient (clones 15–17, Figure 3A), indicating that ZFRs with flexible linkers tended to recombine most efficiently.

ZFR-Catalyzed Recombination in Mammalian Cells. To evaluate the recombination efficiency of ZFR variants in mammalian cells, we constructed a reporter cell line from Flp-In-CHO-K1 containing a cassette that encodes EGFP driven by a CMV promoter flanked by target sites (Figure 4). As each cell contains a single copy of the reporter gene, the recombination efficiency can be calculated from the proportion of cells with or without EGFP fluorescence. Additionally, the expression of ZFR was monitored by the expression of DsRed; this gene was placed downstream of the ZFR gene via a IRES sequence. The genes encoding ZFRs utilized in this study were amplified from a pAra plasmid shown in Figure 2A. Thus, the sequences of clones are the same as those utilized in experiments in *E. coli*.

With this reporter system, recombination efficiencies could be evaluated 48 h after transfection. Reported procedures involving retroviral-based transduction, selection, and evaluation take nearly 10 days.[8] The fluorescence intensity of cells was detected by FACS analysis (Figure S4 of the Supporting Information). The cells with recombinant genes were those that were EGFP-negative and DsRed-positive. The recombination efficiencies depended on the number of finger modules and on the linker lengths (Figure 5). As in *E. coli*, the five-finger proteins were the most efficient in recombination. The optimal linker length was six residues, which is different from that in *E. coli*. Additionally, recombination in mammalian cells was not as efficient as that in *E. coli*.

DISCUSSION

This study demonstrated that ZFR recombinases can be designed to specifically target sites in *E. coli* and mammalian cells and that recombination efficiency depends on the affinity of the ZFP for the DNA target and on the length of the linker between the DNA binding domain and the recombinase domain. The ZFR with five fingers had the highest recombination efficiency in both *E. coli* and CHO-K1 cells. The DNA binding affinity of this particular ZFP was saturated when the DNA binding domain had more than five fingers. The association and dissociation with DNA binding depend on the number of finger modules.[33] It is possible that the ZFR with five fingers was the most efficient recombination because the balance of association with dissociation and turnover was optimal. Guo et al. have also reported that four and five ZF domains are optimal for activity of ZFN.[34] On the basis of our data, the apparent K_d values of the four-, five-, and six-finger proteins derived from this particular ZFP were similar. The dependence on the number of finger modules was common in both *E. coli* and mammalian cells, but the recombination efficiency was lower in mammalian cells. In CHO-K1 cells, DNA is sequestered in chromatin structures. Additionally, the circular form of plasmid DNA could enhance recombination in the bacterial cells.

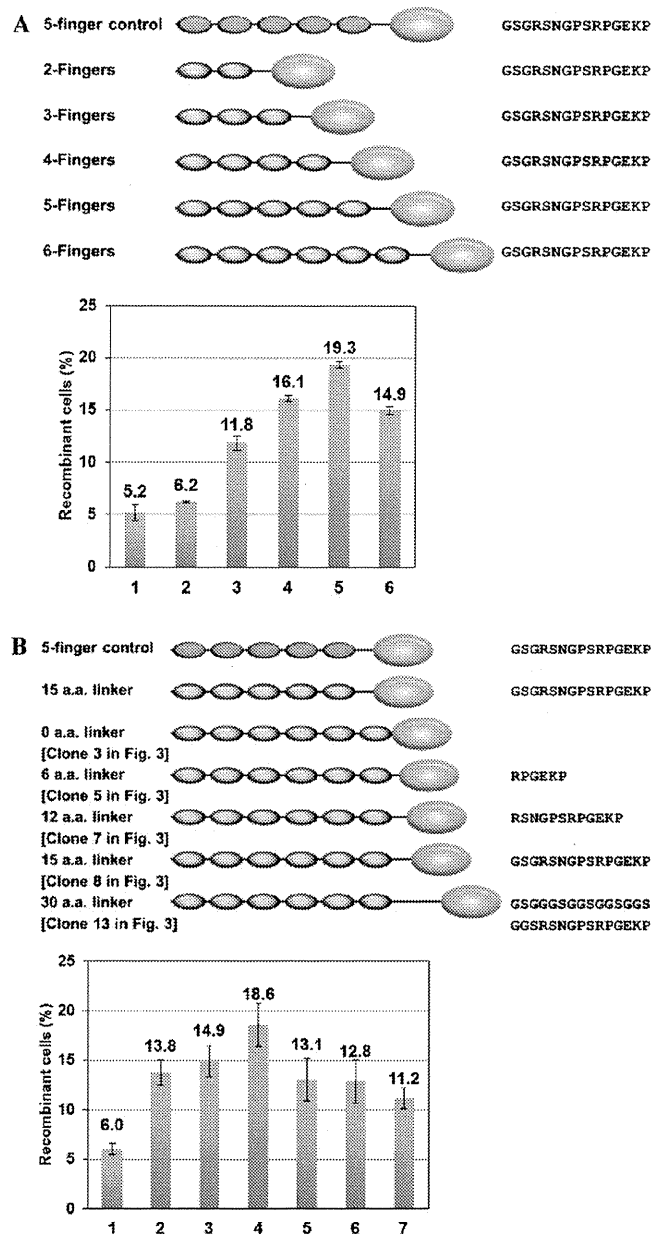

Figure 5. Recombination efficiency of ZFRs containing various numbers of fingers (A) and with various linkers (B) in mammalian cells. The top cartoons represent ZFR constructs utilized in the analyses. Green, blue, and yellow spheres represent zinc finger modules without sequence specificity, zinc finger modules with sequence specificity, and the Tn3 catalytic domain, respectively. Letters at the right of the cartoons are the linker sequences of the constructs. (A) Dependence on the number of fingers of ZFRs. The columns are as follows: column 1, five-finger control (nonspecific DNA binding); column 2, two fingers; column 3, three fingers; column 4, four fingers; column 5, five fingers; column 6, six fingers and different linker lengths. (B) Dependence on linker length. The columns are as follows: column 1, nontarget five-finger control with 15 amino acids; column 2, targeted five-finger ZFR with 15-amino acid linker; columns 3–7, targeted six-finger ZFRs with linker lengths of 0, 6, 12, 15, and 30 amino acids, respectively. The error bars show the SEM of three or more independent experimental results.

Recombination efficiency was dependent on the linker between the zinc finger domain and the recombinase domain. ZFRs with the shortest linkers had a very low efficiency of

dx.doi.org/10.1021/bi201878x | *Biochemistry* XXXX, XXX, XXX–XXX

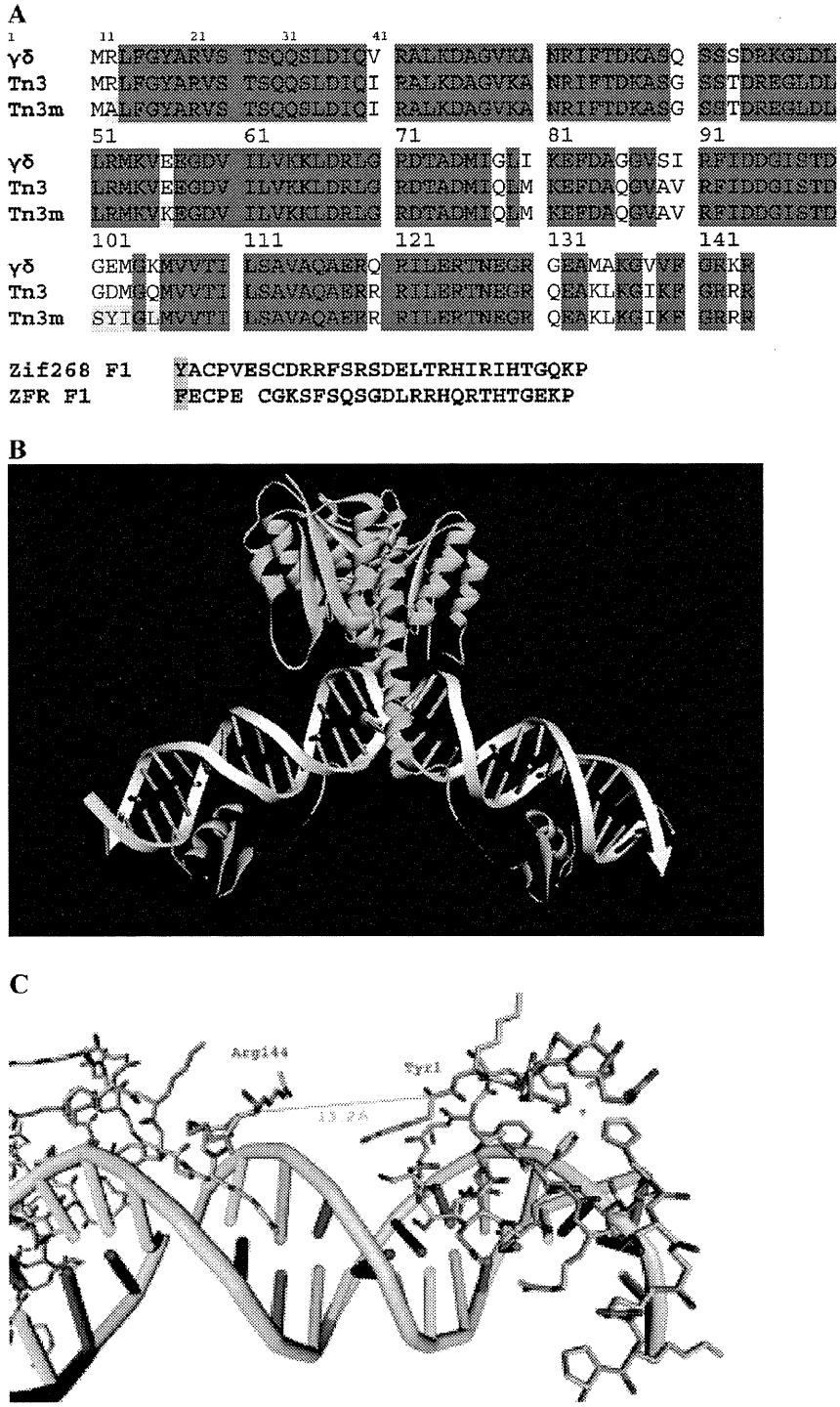

Figure 6. Representative result of molecular modeling of the resolvase domain and the first zinc finger module separated by a six-amino acid linker sequence. (A) Sequence alignment of resolvases $\gamma\delta$ and Tn3 and the Tn3 hyperactivated mutant (Tn3m) (top), the first finger of zif268, and ZFR. Conserved residues are highlighted in red, and amino acid substitutions in the hyperactive mutant are highlighted in yellow. The N-terminal aromatic amino acids of zinc fingers are highlighted in blue. (B) The yellow ribbon indicates $\gamma\delta$ resolvase, the red ribbon the six-amino acid linker, the green ribbon the N-terminal zinc finger domain, and the gray ribbon the zinc ion. (C) Distances between Cα atoms of Arg144 and tyrosine (Tyr) at the N-terminus of zif268. The N-terminal amino acid of the zinc finger domain is phenylalanine (Phe) in ZFRs utilized in this study.

recombination in both bacterial and mammalian cells. Second, the length of linkers based on the original sequences was critical. Proteins with linkers containing 12 amino acid residues were the most efficient in recombination. In the Gly-Ser linker variants, the recombination efficiency reached a maximum at six amino acids. This result indicates that both the length and the flexibility of the linker are important.

A molecular modeling study was performed in an attempt to assess the reasons for the differences in recombination efficiency among the linker mutants. In the modeling of the ZFR complex with target DNA, the linker length of six amino acids was optimal for the DNA binding of ZFR when the linker sequence was flexible (Figure 6A). When the domains were modeled bound to the target sequence, the distance between

dx.doi.org/10.1021/bi201878x | *Biochemistry* XXXX, XXX, XXX–XXX

the Cα atom of Arg144 in the γδ resolvase (Figure S5 of the Supporting Information) and that of Tyr at the N-terminus of the zinc finger domain is ~13.2 Å (Figure 6B,C). In polypeptides in the extended conformation, the distance between Cα atoms of sequential amino acids is 3.8 Å. Thus, a linker consisting of three amino acids (clone 4 or clone 14) should allow the protein to bind to both DNA regions, although these ZFRs had very low recombination efficiencies. In the complex with DNA, the amino groups at positions 145 and 146 of the main chain in γδ resolvase interact with the phosphate backbone of DNA and amino acids of these positions are involved in the folding of the catalytic domain (Figure S5 of the Supporting Information). In the case of clone 4, the Lys-Pro residues at the C-terminus of linker residues are involved in the folding of the zinc finger domain. Thus, these amino acids are considered to be members of both domains, not of the linker sequences. With this reasoning, the six and nine amino acids in the linkers for clones 4 and 5, respectively, are shorter than the theoretically optimal length. Moreover, in the sequences of the six- and nine-amino acid linkers, the amino acid at position 146 is Pro, which could disrupt the interaction with DNA phosphate, thus lowering the recombination efficiency. Consistent with these estimations, the Gly-Ser linker with six or nine amino acids (clones 15 and 16, respectively) showed the best recombination ratio. This evidence indicates that the residues at the C-terminus of the catalytic domain and the N-terminus of the zinc finger domain are involved in domain folding because Lys-Pro residues at the N-terminus of the zinc finger domains are not included in these clones. Variants around this optimal linker length, especially those with 12 and 15 amino acids, had similar recombination efficiencies. These results show that the flexibility of the linker is not necessary when the linker length is optimal. In mammalian cells, the variant with a linker of six amino acids (clone 5) showed the best recombination and the zero-amino acid linker (clone 3) showed better recombination than the variants with longer linkers of more than 12 amino acids. The reason for this effect is unclear, but it could be due to differences in the structures of target sites on the plasmid DNA compared to the genomic DNA. Additionally, the distances between the binding sites in these systems are different. In the genomic target, the binding sites are separated by sequences of more than 2500 bp.

In this study, a newly developed recombination system allowed measurement of recombination efficiencies of ZFRs in *E. coli* and in mammalian cells. In mammalian cells, recombination with genomic targets was evaluated within 48 h of the transient expression of recombinases. Artificial enzymes such as ZFN and ZFR have been studied mainly by using viral vector systems to deliver their genes into mammalian genomes. In a report describing utilization of the retrovirus vectors for gene delivery, the recombination efficiency was as high as ~18%.[8] In our study, we also observed up to 18% recombination in cells. This system could be utilized in future studies to evaluate function of ZFRs on specific targets.

■ ASSOCIATED CONTENT

Supporting Information

Details of subcloning, experimental results of plasmid digestion and sequencing, results of FACS analyses, and a description of key interactions in γδ resolvase. This material is available free of charge via the Internet at http://pubs.acs.org.

■ AUTHOR INFORMATION

Corresponding Author

*E-mail: nomura.mr@tmd.ac.jp or tamamura.mr@tmd.ac.jp. Phone: +81-3-5280-8036. Fax: +81-3-5280-8039.

Funding

This work was supported in part by a Grant-in-Aid for Scientific Research from the Ministry of Education, Culture, Sports, Science and Technology, Japan (20790060), Health and Labor Sciences Research Grants from the Japanese Ministry of Health, Labor, and Welfare, and a grant from the Mochida Memorial Foundation for Medical and Pharmaceutical Research to W.N.

Notes

The authors declare no competing financial interest.

■ REFERENCES

(1) Beerli, R. R., Dreier, B., and Barbas, C. F. III (2000) Positive and negative regulation of endogenous genes by designed transcription factors. *Proc. Natl. Acad. Sci. U.S.A. 97*, 1495–1500.

(2) Pabo, C. O., Peisach, E., and Grant, R. A. (2001) Design and selection of novel Cys2His2 zinc-finger proteins. *Annu. Rev. Biochem. 70*, 313–340.

(3) Beerli, R. R., and Barbas, C. F. III (2002) Engineering polydactyl zinc-finger transcription factors. *Nat. Biotechnol. 20*, 135–141.

(4) Jamieson, A. C., Miller, J. C., and Pabo, C. O. (2003) Drug discovery with engineered zinc-finger proteins. *Nat. Rev. Drug Discovery 2*, 361–368.

(5) Blancafort, P., Segal, D. J., and Barbas, C. F. III (2004) Designing transcription factor architectures for drug discovery. *Mol. Pharmacol. 66*, 1361–1371.

(6) Carroll, D. (2008) Progress and prospects: Zinc-finger nucleases as gene therapy agents. *Gene Ther. 15*, 1463–1468.

(7) Akopian, A., He, J., Boocock, M. R., and Stark, W. M. (2003) Chimeric recombinases with designed DNA sequence recognition. *Proc. Natl. Acad. Sci. U.S.A. 100*, 8688–8691.

(8) Gordley, R. M., Smith, J. D., Gräslund, T., and Barbas, C. F. III (2007) Evolution of programmable zinc-finger-recombinases with activity in human cells. *J. Mol. Biol. 367*, 802–813.

(9) Gordley, R. M., Gersbach, C. A., and Barbas, C. F. III (2009) Synthesis of programmable integrases. *Proc. Natl. Acad. Sci. U.S.A. 106*, 5053–5058.

(10) Gersbach, C. A., Gaj, T., Gordley, R. M., and Barbas, C. F. III (2010) Directed evolution of recombinase specificity by split gene reassembly. *Nucleic Acids Res. 38*, 4198–4206.

(11) Gaj, T., Mercer, A. C., Gersbach, C. A., Gordley, R. M., and Barbas, C. F. III (2011) Structure-Guided Reprogramming of Serine Recombinase DNA Sequence Specificity. *Proc. Natl. Acad. Sci. U.S.A. 108*, 498–503.

(12) Gersbach, C. A., Gaj, T., Gordley, R. M., Mercer, A. C., and Barbas, C. F. III (2011) Targeted plasmid integration into the human genome by an engineered zinc-finger recombines. *Nucleic Acids Res. 39*, 7868–7878.

(13) Xu, G.-L., and Bestor, T. H. (1997) Cytosine methylation targeted to predetermined sequences. *Nat. Genet. 17*, 376–378.

(14) McNamara, A. R., Hurd, P. J., Smith, A. E., and Ford, K. G. (2002) Characterisation of site-biased DNA methyltransferases: Specificity, affinity and subsite relationships. *Nucleic Acids Res. 30*, 3818–3130.

(15) Carvin, C. D., Parr, R. D., and Kladde, M. P. (2003) Site-selective in vivo targeting of cytosine-5 DNA methylation by zinc-finger proteins. *Nucleic Acids Res. 31*, 6493–6501.

(16) Minczuk, M., Papworth, M. A., Kolasinska, P., Murphy, M. P., and Klug, A. (2006) Sequence-specific modification of mitochondrial DNA using a chimeric zinc-finger methylase. *Proc. Natl. Acad. Sci. U.S.A. 103*, 19689–19694.

(17) Li, F., Papworth, M., Minczuk, M., Rohde, C., Zhang, Y., Ragozin, S., and Jeltsch, A. (2007) Chimeric DNA methyltransferases

target DNA methylation to specific DNA sequences and repress expression of target genes. *Nucleic Acids Res. 35*, 100−112.
(18) Smith, A. E., and Ford, K. G. (2007) Specific targeting of cytosine methylation to DNA sequences in vivo. *Nucleic Acids Res. 35*, 740−754.
(19) Smith, A. E., Hurd, P. J., Bannister, A. J., Kouzarides, T., and Ford, K. G. (2008) Heritable Gene Repression through the Action of a Directed DNA Methyltransferase at a Chromosomal Locus. *J. Biol. Chem. 283*, 9878−9885.
(20) Nomura, W., and Barbas, C. F. III (2007) In vivo site-specific DNA methylation with a designed sequence-enabled DNA methylase. *J. Am. Chem. Soc. 129*, 8676−8677.
(21) Grindley, N. D., Whiteson, K. L., and Rice, P. A. (2006) Mechanisms of site-specific recombination. *Annu. Rev. Biochem. 75*, 567−605.
(22) Yang, W., and Steitz, T. A. (1995) Crystal structure of the site-specific recombinase gamma delta resolvase complexed with a 34 bp cleavage site. *Cell 82*, 193−207.
(23) Arnold, P. H., Blake, D. G., Grindley, N. D., Boocock, M. R., and Stark, W. M. (1999) Mutants of Tn3 resolvase which do not require accessory binding sites for recombination activity. *EMBO J. 18*, 1407−1414.
(24) Li, W., Kamtekar, S., Xiong, Y., Sarkis, G. J., Grindley, N. D., and Steitz, T. A. (2005) Structure of a synaptic $\gamma\delta$ resolvase tetramer covalently linked to two cleaved DNAs. *Science 309*, 1210−1215.
(25) Olorunniji, F. J., He, J., Wenwieser, S. V., Boocock, M. R., and Stark, W. M. (2008) Synapsis and catalysis by activated Tn3 resolvase mutants. *Nucleic Acids Res. 36*, 7181−7191.
(26) Gonzalez, B., Schwimmer, L. J., Fuller, R. P., Ye, Y., Asawapornmongkol, L., and Barbas, C. F. III (2010) Modular system for the construction of zinc-finger libraries and proteins. *Nat. Protoc. 5*, 791−810.
(27) Mandell, J. G., and Barbas, C. F. III (2006) Zinc Finger Tools: Custom DNA-binding domains for transcription factors and nucleases. *Nucleic Acids Res. 34*, W516−W523.
(28) Kim, C. A., and Berg, J. M. (1996) A 2.2 Angstroms resolution crystal structure of a designed zinc finger protein bound to DNA. *Nat. Struct. Mol. Biol. 3*, 940−945.
(29) Segal, D. J., Dreier, B., Beerli, R. R., and Barbas, C. F. III (1999) Toward controlling gene expression at will: Selection and design of zinc finger domains recognizing each of the 5′-GNN-3′ DNA target sequences. *Proc. Natl. Acad. Sci. U.S.A. 96*, 2758−2763.
(30) Dreier, B., Segal, D. J., and Barbas, C. F. III (2000) Insights into the molecular recognition of the 5′-GNN-3′ family of DNA sequences by zinc-finger domains. *J. Mol. Biol. 303*, 489−502.
(31) Dreier, B., Beerli, R. R., Segal, D. J., Flippin, J. D., and Barbas, C. F. III (2001) Development of zinc finger domains for recognition of the 5′-ANN-3′ family of DNA sequences and their use in the construction of artificial transcription factors. *J. Biol. Chem. 276*, 29466−29478.
(32) Dreier, B., Fuller, R. P., Segal, D. J., Lund, C., Blancafort, P., Huber, A., Koksch, B., and Barbas, C. F. III (2005) Development of zinc finger domains for recognition of the 5′-CNN-3′ family DNA sequences and their use in the construction of artificial transcription factors. *J. Biol. Chem. 280*, 35588−35597.
(33) Kamiuchi, T., Abe, E., Imanishi, M., Kaji, T., Nagaoka, M., and Sugiura, Y. (1998) Artificial nine zinc-finger peptide with 30 base pair binding sites. *Biochemistry 37*, 13827−13834.
(34) Guo, J., Gaj, T., and Barbas, C. F. III (2010) Directed evolution of an enhanced and highly efficient FokI cleavage domain for zinc finger nuclease. *J. Mol. Biol. 400*, 96−107.

DOI: 10.1002/cmdc.201100542

A Synthetic C34 Trimer of HIV-1 gp41 Shows Significant Increase in Inhibition Potency

Wataru Nomura,[a] Chie Hashimoto,[a] Aki Ohya,[a] Kosuke Miyauchi,[b] Emiko Urano,[b] Tomohiro Tanaka,[a] Tetsuo Narumi,[a] Toru Nakahara,[a] Jun A. Komano,[b] Naoki Yamamoto,[c] and Hirokazu Tamamura*[a]

The development of new anti-HIV-1 drugs such as inhibitors of protease and integrase has been contributed to highly active anti-retroviral therapy (HAART) for the treatment of AIDS.[1] The entry of human immunodeficiency virus type 1 (HIV-1) into target cells is mediated by its envelope glycoprotein (Env), a type I transmembrane protein that consists of surface subunit gp120 and noncovalently associated transmembrane subunit gp41.[2] Sequential binding of HIV-1 gp120 to its cell receptor CD4 and a co-receptor (CCR5 or CXCR4) can trigger a series of conformational rearrangements in gp41 to mediate fusion between viral and cellular membranes.[3–5] The protein gp41 is hidden beneath gp120, and its ectodomain contains helical N- and C-terminal leucine/isoleucine heptad repeat domains, N-HR and C-HR. Particular regions of N-HR and C-HR are involved in membrane fusion, and 36-mer and 34-mer peptides, which are derived from N-HR and C-HR, have been designated as the N-terminal helix (N36) and C-terminal helix (C34), respectively. In the membrane fusion of HIV-1, these helices assemble to form a six-helical bundle (6-HB) consisting of a central parallel trimer of N36 surrounded by C34 in an antiparallel hairpin fashion. Synthetic peptides derived from these helices have potent antiviral activity against both laboratory-adapted strains and primary isolates of HIV-1.[6–9] They inhibit the membrane fusion stage of HIV-1 infection in a dominant-negative manner by binding to the counterpart regions of gp41 (N-HR or C-HR), blocking formation of the viral gp41 core.

Several potent anti-HIV-1 peptides based on the C-HR region have been discovered,[7,8] and T20 was subsequently developed as the clinical anti-HIV-1 drug enfuvirtide (Roche/Trimeris).[8,10–13] It is a 36-mer peptide derived from the gp41 C-HR sequence and can bind to the N-HR to prevent formation of the 6-HB in a dominant-negative fashion.[10] T20 therapy has brought safety, potent antiretroviral activity, and immunological benefit to patients, but its clinical application is limited by the development of resistance. The C-terminal helix C34 is also a C-HR-derived peptide, and contains the amino acid residues required for docking into the hydrophobic pocket, termed the "deep pocket", of the trimer of the N-HR region. This peptide potently inhibits HIV-1 fusion in vitro.[14] To date, several gp41 mimetics, especially those of N36 regions, which assemble these helical peptides with branched peptide linkers, have been synthesized as antigens.[15–19]

Recently, by using a novel template with C3-symmetric linkers of equal length, we synthesized a three-helix bundle mimetic that corresponds to the trimeric form of N36.[20] The antisera obtained from mice immunized by the peptide antigen showed strong recognition against the N36 trimer peptide with structural preference. At the same time, the trimer peptide was also investigated as a fusion inhibitor. However, the trimer N36 showed only a threefold increase in inhibition of HIV-1 fusion relative to the N36 monomer.[20] In terms of N36 content, the trimer and monomer have nearly the same inhibitory potency. This phenomenon is consistent with the results from other studies.[21–23] The multimerization of the functional unit, such as synthetic ligands against receptors, show synergistic binding and strong binding activity. Thus, we hypothesized that our strategy using C3-symmetric linkers in the design of trimer mimics of gp41 could be applied to the C34 peptide, which shows significant inhibition potency in the monomeric form. In the present study, we designed and synthesized a novel three-helical bundle structure of the trimeric form of C34. This equivalent mimic of the trimeric form of C34 was evaluated as a novel form of fusion inhibitor.

The C-terminal region of gp41 is known to be an assembly site involving a trimeric coiled-coil conformation. In the design of the C34-derived peptides C34REG-thioester (Figure 1 A) and C34REG (Figure 1 B), the triplet repeat of arginine and glutamic acid (RERERE) was added to the C-terminal end of the C34 sequence (residues 628–661) to increase aqueous solubility, and for C34REG-thioester, a glycine thioester was fused to the C terminus. To form a triple helix corresponding precisely to the gp41 pre-fusion form, we designed the novel C3-symmetric template depicted in Figure 1 C. This designed template linker has three branches of equal length, a hydrophilic structure, and a ligation site for coupling with C34REG-thioester. The template was synthesized as shown in Scheme 1. This approach uses native chemical ligation for chemoselective coupling of unprotected C34REG-thioester with a three-armed cysteine scaffold to produce triC34e (Figure 2).[24,25]

Circular dichroism (CD) spectra of C34REG and triC34e are shown in Figure 3 A. The peptides were dissolved in 50 mM sodium phosphate buffer with 150 mM NaCl, pH 7.2. Both spectra display minima at ~200 nm, indicating that these peptides form random structures. We previously reported that the

[a] Dr. W. Nomura, C. Hashimoto, A. Ohya, Dr. T. Tanaka, Dr. T. Narumi, T. Nakahara, Prof. Dr. H. Tamamura
Institute of Biomaterials and Bioengineering
Tokyo Medical and Dental University
2-3-10 Kandasurugadai, Chiyoda-ku, Tokyo 101-0062 (Japan)
E-mail: tamamura.mr@tmd.ac.jp

[b] Dr. K. Miyauchi, Dr. E. Urano, Dr. J. A. Komano
AIDS Research Center, National Institute of Infectious Diseases
1-23-1 Toyama, Shinjuku-ku, Tokyo 162-8640 (Japan)

[c] Prof. Dr. N. Yamamoto
Department of Microbiology, Yong Loo Lin School of Medicine
National University of Singapore
5 Science Drive 2, Singapore 117597 (Singapore)

Supporting information for this article is available on the WWW under http://dx.doi.org/10.1002/cmdc.201100542.

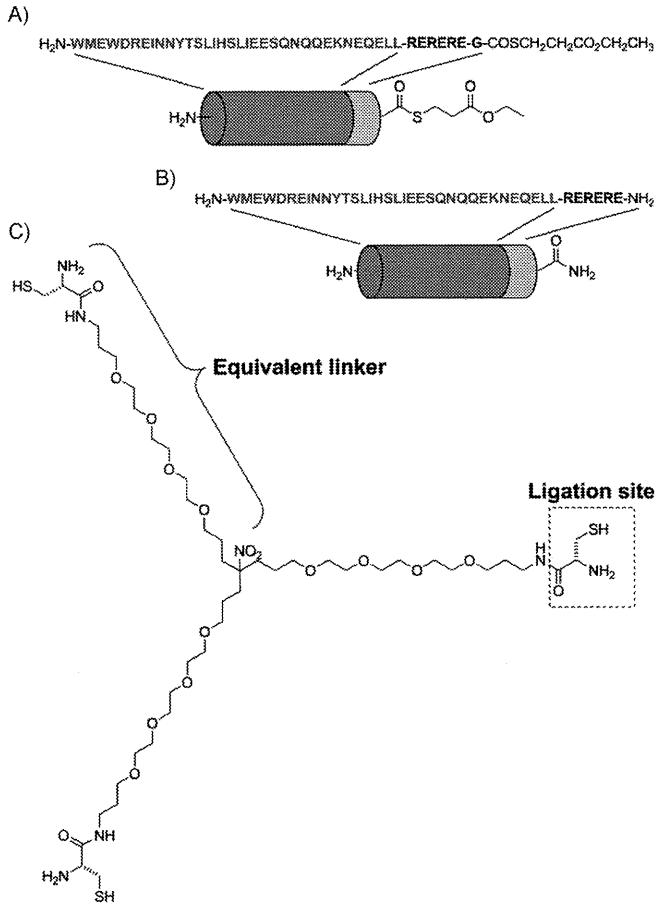

Figure 1. C34-derived peptides: A) C34REG-thioester and B) C34REG. C) The design of a C3-symmetric template.

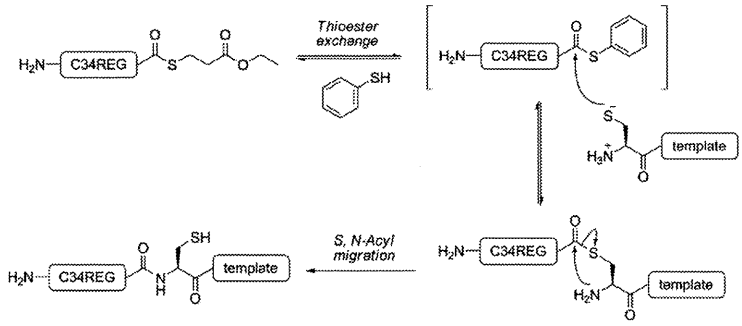

Figure 2. The native chemical ligation used for assembly of the C34REG-thioester on the template.

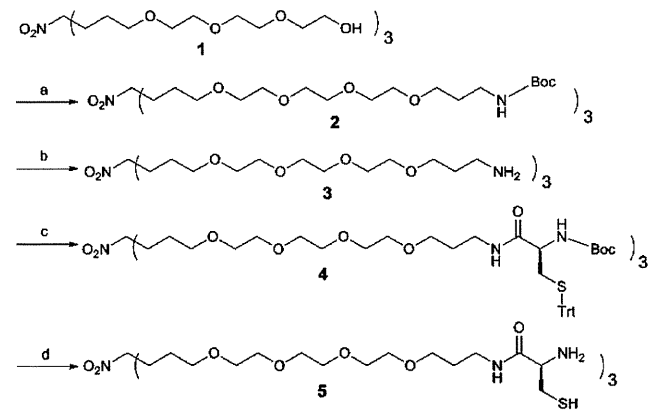

Scheme 1. Synthesis of the equivalently branched template **5**. *Reagents and conditions*: a) (3-bromopropyl)carbamic acid *tert*-butyl ester, NaH, THF; b) 4 M HCl/dioxane; c) Boc-Cys(Trt)-OH, EDCI·HCl, HOBt·H_2O, Et_3N, DMF; d) 90% aq. TFA.

helical content of the trimer triC34e and N36RE mixture is lower than that of the monomer C34REG and N36RE mixture. This is evidence that relative to the monomer C34REG, the trimer triC34e interacts with N36 only with difficulty, due to the assembly of three peptide strands by covalent bonds.

As the trimeric C34 was proven to interact with N36 helices, the potential HIV-1 inhibitory activities of the C-terminal peptides, C34REG and triC34e, were evaluated. The C34 peptide without the solubility-increasing sequence (3×[Arg-Glu], obtained from NIAID) was used as the monomeric control.[27] All peptides showed potent inhibitory activity in the viral fusion assay (Table 1), with the potency of triC34e being 100- and 40-fold higher than that of C34REG and C34 peptides, respectively. Notably, the triC34e trimer peptide is remarkably more potent in anti-HIV-1 activity than the monomer, indicating that a trimeric form is critical for inhibitory activity. Cytotoxicity from the peptides was not observed at concentrations of 15 μM for C34REG and C34, and 5 μM for triC34e.

We next carried out an assay for the inhibition of viral replication. As shown in Table 2, triC34e showed 30- and 20-fold higher inhibitory activity than peptides C34 and C34REG, respectively. In the two anti-HIV-1 assays, triC34e showed a great enhancement of activity over the C34 monomers. The IC_{50} values obtained in the assays are different, and this can be

N36 monomer N36RE and the N36 trimer triN36e form a highly structured α helix, and that the helical content of triN36e was greater than that of N36RE.[20,26] These results suggest that in contrast to N36-derived peptides, C34-derived peptides tend to form random structures both in the monomeric and trimeric forms. To assess the interaction of triC34e with N36, CD spectra of a mixture of triC34e with an N36-derived peptide, N36RE, were measured (Figure 3 B). The spectrum of the C34REG and N36RE mixture and that of the triC34e and N36RE mixture showed double minima at λ 208 and 222 nm, indicating that the peptide mixture forms an α-helical structure and that the

Table 1. IC_{50} and CC_{50} values determined by viral fusion inhibition and cell viability assays.

	C34 peptide[a]	C34REG	triC34e
IC_{50} [μM][b]	0.044	0.12	0.0013
CC_{50} [μM][c]	>15	>15	>5

[a] HIV-1 IIIB C34 peptide. [b] IC_{50} values are based on luciferase signals in TZM-bl cells infected with HIV-1 (NL4-3 strain). [c] CC_{50} values are based on the decrease in viability of TZM-bl cells. All data are the mean values from at least three experiments.

Table 2. IC_{50} values determined by inhibition assay based on p24 ELISA.			
	C34 peptide	C34REG	triC34e
IC_{50} [μM][a]	1.59	1.06	0.0547
[a] IC_{50} values are based on the production of p24 in MT-4 cells infected with HIV-1 (NL4-3 strain). All data are the mean values from at least three experiments.			

explained through differences in experimental procedures. In the fusion inhibition assay, cells were treated with peptides before viral infection. In contrast, in the viral replication inhibition assay, peptides were treated after viral adsorption to cells. Therefore, in the latter case, the infection by HIV-1 might precede peptide binding to gp41.

It has been shown that T-1249, an analogue of enfuvirtide, and its hydrophobic C-terminal region inhibit HIV-1 fusion by interacting with lipid bilayers.[28] The tryptophan-rich domain of T-1249 was shown to play important roles in HIV-1 fusion.[29–31] As enfuvirtide shows weak interaction with the gp41 core structure, and the C34 sequence lacks the C-terminal lipid binding domain, it has been suggested that C34 has a mechanism of action distinct from that of enfuvirtide.[32] Thus, it is of interest to discern the mechanism of the enhanced inhibition observed with triC34e relative to the monomer. Two explanations can be envisaged: 1) the α helicity of the C34 trimer is higher than that of the monomer, as shown in Figure 3A, and as a result, the C34 trimer binds more strongly to the N36 trimer; and 2) in the mixture with the N36 monomer, the C34 trimer shows less α helicity than its monomer (Figure 3B). As shown in Figure 3A, the molar ellipticity at 222 nm is similar for both the C34 trimer and the monomer. Thus, the decrease at 222 nm in the mixture with N36 might be due to a decrease in the α helicity of N36. These results suggest that the C34 trimer might destabilize helix formation in N36 and thus exert potent inhibitory activity. It has been shown that a dimeric C37 (residues 625–661) variant does not show a significant difference in IC_{50} value against HIV-1 from wild-type C37, although the dimeric peptide shows tighter binding to the gp41 N-HR coiled-coil than the C37 monomer.[33] Thus, the mechanism of action of the C34 trimer could be different from that of the dimeric C-peptide. The detailed action mechanism of the trimer as a fusion inhibitor and the reasons behind its remarkable increased anti-HIV-1 activity will be the subjects of future studies in our research group.

A C-terminal helical peptide of HIV-1 gp41 has been designed as a new HIV fusion inhibitor and was synthesized with a novel template and three branched linkers of equal length. The native chemical ligation proceeded by chemoselective coupling in an aqueous medium of an unprotected C34 derivative containing a C-terminal thioester with a three-cysteine-armed scaffold. This process led to the production of triC34e. As a fusion inhibitor, triC34e has potent anti-HIV-1 activity, 100-fold greater than that of the C34REG monomer, although the anti-HIV-1 activity of the N36 trimer is threefold higher than that of the N36 monomer, and the N36 content is the same in both cases.[20] A trimeric form of C34 is evidently critical as the active structure of the fusion inhibitor. The soluble C34 derivative, SC34, retains potent inhibitory effects against enfuvirtide-resistant viruses,[34] and this suggests that the present highly potent trimeric inhibitor could be effective for enfuvirtide-resistant HIV-1 strains. The design of inhibitors that target the dynamic supramolecular mechanism of HIV-1 fusion will be useful for future studies of anti-HIV-1 agents.

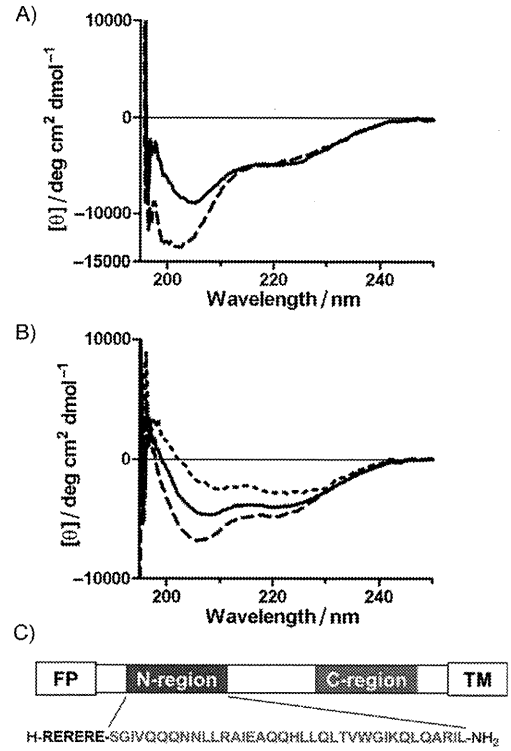

Figure 3. A) CD spectra of C34REG (monomer, -----, 6 μM) and triC34e (trimer, ——, 2 μM). B) CD spectra in the presence or absence of the N36 monomer N36RE:[20] -----, [C34REG (6 μM) + N36RE (6 μM)]; ——, [triC34e (2 μM) + N36RE (6 μM)]; •••••, N36RE (6 μM). In the amino acid sequence of N36RE, the triplet repeat of arginine and glutamic acid is located at the N-terminus of the original N36 sequence.[20] C) Amino acid sequence of N36RE: FP and TM represent the hydrophobic fusion peptide and transmembrane domains, respectively.

Experimental Section

Conjugation of C34REG-thioester and the template to produce triC34e

TCEP·HCl (773 μg, 2.67 μmol) and thiophenol (9 μL, 89 μmol) were dissolved in 0.1 M sodium phosphate buffer (60 μL) containing 6 M urea and EDTA (pH 8.5, 2 mM) under a nitrogen atmosphere. Compound **5** (100 μg, 0.0899 μmol), C34REG-thioester (1.77 mg, 0.297 μmol), and CH_3CN (20 μL) were added. The reaction was stirred for 5 h at 37 °C and monitored by HPLC. The ligation product (triC34e) was separated as an HPLC peak and characterized by ESI-ToF-MS (*m/z* calcd for $C_{703}H_{1108}N_{205}O_{245}S_6$ $[M+H]^+$: 16533.9, found: 16543.8). Purification was performed by reversed-phase HPLC (Cosmosil 5 C_{18}-AR II column, 10×250 mm, Nacalai Tesque, Inc.) with elution using a 33–43% linear gradient of CH_3CN (0.1% TFA) over 40 min. Purified triC34e, obtained in 17% yield, was identified by ESI-ToF-MS. Details of the synthesis of these peptides are described in the Supporting Information.

CD spectra

Circular dichroism measurements were performed with a J-720 CD spectropolarimeter equipped with a thermoregulator (Jasco). The wavelength dependence of molar ellipticity [θ] was monitored at 25 °C from λ 195 to 250 nm. The peptides were dissolved in PBS (50 mM sodium phosphate, 150 mM NaCl, pH 7.2).

Virus preparation

For virus preparation, 293FT cells in a 60 mm dish were transfected with the pNL4-3 construct (10 μg) by the calcium phosphate method. The supernatant was collected 48 h after transfection, passed through a 0.45 μm filter, and stored at −80 °C as the virus stock.

Anti-HIV-1 assay

For the viral fusion inhibition assay, TZM-bl cells (2×10^4 cells per 100 μL) were cultured with the NL4-3 virus (5 ng of p24) and serially diluted peptides. After culture for 48 h, cells were lysed, and the luciferase activity was determined with the Steady-Glo luciferase assay system (Promega, Fitchburg, WI, USA).[35] For the viral replication inhibition assay, MT-4 cells (5×10^4 cells) were exposed to HIV-1 NL4-3 (1 ng of p24) at 4 °C for 30 min. After centrifugation, cells were resuspended with 150 μL medium containing indicated concentrations of serially diluted peptides. Cells were cultured at 37 °C for 3 days, and the concentration of p24 in the culture supernatant was determined by HIV-1 p24 antigen ELISA kit (ZeptoMetrix, Buffalo, NY, USA).

Cytotoxicity assay

The cytotoxic effects of peptides were determined by the CellTiter 96 AQueous One Solution Cell Proliferation assay system (Promega) under the same conditions, but in the absence of viral infection.

Acknowledgements

The following reagent was obtained through the US National Institutes of Health (NIH) AIDS Research and Reference Reagent Program, Division of AIDS, NIAID, NIH: HIV-1 IIIB C34 Peptide from DAIDS, NIAID. This work was supported in part by a Grant-in-Aid for Scientific Research from the Ministry of Education, Culture, Sports, Science, and Technology of Japan, and Health and Labour Sciences Research Grants from the Japanese Ministry of Health, Labor, and Welfare. C.H. is supported by JSPS research fellowships for young scientists.

Keywords: antiviral agents · C34 trimers · fusion inhibitors · gp41 · HIV-1

[1] C. Hashimoto, T. Tanaka, T. Narumi, W. Nomura, H. Tamamura, *Expert Opin. Drug Discovery* **2011**, *6*, 1067–1090.
[2] E. O. Freed, M. A. Martin, *J. Biol. Chem.* **1995**, *270*, 23883–23886.
[3] D. M. Eckert, P. S. Kim, *Annu. Rev. Biochem.* **2001**, *70*, 777–810.
[4] R. Wyatt, J. Sodroski, *Science* **1998**, *280*, 1884–1888.
[5] E. A. Berger, P. M. Murphy, J. M. Farber, *Annu. Rev. Immunol.* **1999**, *17*, 657–700.
[6] M. Lu, S. C. Blacklow, P. S. Kim, *Nat. Struct. Biol.* **1995**, *2*, 1075–1082.
[7] S. Jiang, K. Lin, N. Strick, A. R. Neurath, *Nature* **1993**, *365*, 113.
[8] C. T. Wild, D. C. Shugars, T. K. Greenwell, C. B. McDanal, T. J. Matthews, *Proc. Natl. Acad. Sci. USA* **1994**, *91*, 9770–9774.
[9] C. T. Wild, T. Oas, C. McDanal, D. Bolognesi, T. Matthews, *Proc. Natl. Acad. Sci. USA* **1992**, *89*, 10537–10541.
[10] J. M. Kilby, S. Hopkins, T. M. Venetta, B. DiMassimo, G. A. Cloud, J. Y. Lee, L. Alldredge, E. Hunter, D. Lambert, D. Bolognesi, T. Matthews, M. R. Johnson, M. A. Nowak, G. M. Shaw, M. S. Saag, *Nat. Med.* **1998**, *4*, 1302–1307.
[11] J. M. Kilby, J. J. Eron, *N. Engl. J. Med.* **2003**, *348*, 2228–2238.
[12] J. P. Lalezari, K. Henry, M. O'Hearn, J. S. Montaner, P. J. Piliero, B. Trottier, S. Walmsley, C. Cohen, D. R. Kuritzkes, J. J. Eron, Jr., J. Chung, R. DeMasi, L. Donatacci, C. Drobnes, J. Delehanty, M. Salgo, *N. Engl. J. Med.* **2003**, *348*, 2175–2185.
[13] S. Liu, W. Jing, B. Cheng, H. Lu, J. Sun, X. Yan, J. Niu, J. Farmar, S. Wu, S. Jiang, *J. Biol. Chem.* **2007**, *282*, 9612–9620.
[14] D. C. Chan, D. Fass, J. M. Berger, P. S. Kim, *Cell* **1997**, *89*, 263–273.
[15] E. De Rosny, R. Vassell, R. T. Wingfield, C. T. Wild, C. D. Weiss, *J. Virol.* **2001**, *75*, 8859–8863.
[16] J. P. Tam, Q. Yu, *Org. Lett.* **2002**, *4*, 4167–4170.
[17] W. Xu, J. W. Taylor, *Chem. Biol. Drug Des.* **2007**, *70*, 319–328.
[18] J. M. Louis, I. Nesheiwat, L. Chang, G. M. Clore, C. A. Bewlet, *J. Biol. Chem.* **2003**, *278*, 20278–20285.
[19] E. Bianch, J. G. Joyce, M. D. Miller, A. C. Finnefrock, X. Liang, M. Finotto, P. Ingllinella, P. McKenna, M. Citron, E. Ottinger, R. W. Hepler, R. Hrin, D. Nahas, C. Wu, D. Montefiori, J. W. Shiver, A. Pessi, P. S. Kim, *Proc. Natl. Acad. Sci. USA* **2010**, *107*, 10655–10660.
[20] T. Nakahara, W. Nomura, K. Ohba, A. Ohya, T. Tanaka, C. Hashimoto, T. Narumi, T. Murakami, N. Yamamoto, H. Tamamura, *Bioconjugate Chem.* **2010**, *21*, 709–714.
[21] M. Lu, H. Ji, S. Shen, *J. Virol.* **1999**, *73*, 4433–4438.
[22] D. M. Eckert, P. S. Kim, *Proc. Natl. Acad. Sci. USA* **2001**, *98*, 11187–11192.
[23] E. Bianchi, M. Finotto, P. Ingallinella, R. Hrin, A. V. Carella, X. S. Hous, W. A. Schleif, M. D. Miller, *Proc. Natl. Acad. Sci. USA* **2005**, *102*, 12903–12908.
[24] P. E. Dawson, T. W. Muir, I. Clark-Lewis, S. B. H. Kent, *Science* **1994**, *266*, 776–779.
[25] P. E. Dawson, M. J. Churchill, M. R. Ghadiri, S. B. H. Kent, *J. Am. Chem. Soc.* **1997**, *119*, 4325–4329.
[26] D. C. Chan, C. T. Chutkowski, P. S. Kim, *Proc. Natl. Acad. Sci. USA* **1998**, *95*, 15613–15617.
[27] S. A. Gallo, K. Sackett, S. S. Rawat, Y. Shai, R. Blumenthal, *J. Mol. Biol.* **2004**, *340*, 9–14.
[28] A. S. Veiga, N. C. Santos, L. M. Loura, A. Fedorov, M. A. Castanho, *J. Am. Chem. Soc.* **2004**, *126*, 14758–14763.
[29] M. K. Lawless, S. Barney, K. I. Guthrie, T. B. Bucy, S. R. Petteway, Jr., G. Merutka, *Biochemistry* **1996**, *35*, 13697–13708.
[30] K. Salzwedel, J. T. West, E. Hunter, *J. Virol.* **1999**, *73*, 2469–2480.
[31] S. G. Peisajovich, S. A. Gallo, R. Blumenthal, Y. Shai, *J. Biol. Chem.* **2003**, *278*, 21012–21017.
[32] S. Liu, H. Lu, Y. Xu, S. Wu, S. Jiang, *J. Biol. Chem.* **2005**, *280*, 11259–11273.
[33] K. M. Kahle, K. Steger, M. J. Root, *PLoS Pathog.* **2009**, *5*, e1000674.
[34] A. Otaka, M. Nakamura, D. Nameki, E. Kodama, S. Uchiyama, S. Nakamura, H. Nakano, H. Tamamura, Y. Kobayashi, M. Matsuoka, N. Fujii, *Angew. Chem.* **2002**, *114*, 3061–3064; *Angew. Chem. Int. Ed.* **2002**, *41*, 2937–2940.
[35] E. J. Platt, K. Wehrly, S. E. Kuhmann, B. Chesebro, D. Kabat, *J. Virol.* **1998**, *72*, 2855–2864.

Received: November 22, 2011
Revised: December 15, 2011
Published online on January 13, 2012

Bioorganic & Medicinal Chemistry 20 (2012) 1468–1474

Contents lists available at SciVerse ScienceDirect

Bioorganic & Medicinal Chemistry

journal homepage: www.elsevier.com/locate/bmc

Conjugation of cell-penetrating peptides leads to identification of anti-HIV peptides from matrix proteins

Tetsuo Narumi [a], Mao Komoriya [a], Chie Hashimoto [a], Honggui Wu [b,c], Wataru Nomura [a], Shintaro Suzuki [a], Tomohiro Tanaka [a], Joe Chiba [c], Naoki Yamamoto [d], Tsutomu Murakami [b,*], Hirokazu Tamamura [a,*]

[a] Institute of Biomaterials and Bioengineering, Tokyo Medical and Dental University, Chiyoda-ku, Tokyo 101-0062, Japan
[b] AIDS Research Center, National Institute of Infectious Diseases, Shinjuku-ku, Tokyo 162-8640, Japan
[c] Department of Biological Science Technology, Tokyo University of Science, Noda, Chiba 278-8510, Japan
[d] Yong Loo Lin School of Medicine, National University of Singapore, Singapore 117597, Singapore

ARTICLE INFO

Article history:
Received 6 December 2011
Revised 24 December 2011
Accepted 24 December 2011
Available online 2 January 2012

Keywords:
Matrix protein
Octa-arginyl group
Overlapping peptide
Anti-HIV

ABSTRACT

Compounds which inhibit the HIV-1 replication cycle have been found amongst fragment peptides derived from an HIV-1 matrix (MA) protein. Overlapping peptide libraries covering the whole sequence of MA were designed and constructed with the addition of an octa-arginyl group to increase their cell membrane permeability. Imaging experiments with fluorescent-labeled peptides demonstrated these peptides with an octa-arginyl group can penetrate cell membranes. The fusion of an octa-arginyl group was proven to be an efficient way to find active peptides in cells such as HIV-inhibitory peptides.

1. Introduction

Several anti-retroviral drugs beyond reverse transcriptase inhibitors, including effective protease inhibitors[1] and integrase inhibitors[2,3] are currently available to treat human immunodeficiency virus type 1 (HIV-1) infected individuals. We have also developed several anti-HIV agents such as coreceptor CXCR4 antagonists,[4–7] CD4 mimics,[8–10] fusion inhibitors[11] and integrase inhibitors.[12,13] However, the emergence of viral strains with multi-drug resistance (MDR), which accompanies the development of any antiviral drug, has encouraged a search for new types of anti-HIV-1 drugs with different inhibitory mechanisms.

Matrix (MA) proteins are essential for assembly of the virion shell. MA is a component of the Gag precursor protein, Pr55Gag, and is located within the viral membrane.[14,15] It has been reported that MA-derived peptides such as MA(47–59) inhibit infection by HIV,[16] and that MA-derived peptides such as MA(31–45) and MA(41–55) show anti-HIV activity.[17] In addition, Morikawa et al. report that MA(61–75) and MA(71–85) inhibit MA dimerization, a necessary step in the formation of the virion shell.[18] However, the question of whether the above MA peptides can penetrate cell membranes was not addressed in these reports. We speculate that to achieve antiviral activity it is essential that the MA-derived peptides penetrate the cell membrane and function intracellularly. In this paper, we report our design and construction of an overlapping library of fragment peptides derived from the MA protein with a cell membrane permeable signal. Our aim is the discovery of potent lead compounds, which demonstrate HIV inhibitory activity inside the host cells.

2. Materials and methods

2.1. Peptide synthesis

MA-derived fragments and an octa-arginyl (R_8) peptide were synthesized by stepwise elongation techniques of Fmoc-protected amino acids on a Rink amide resin. Coupling reactions were performed using 5.0 equiv of Fmoc-protected amino acid, 5.0 equiv of diisopropylcarbodiimide and 5.0 equiv of 1-hydroxybenzotriazole monohydrate. Ac_2O–pyridine (1/1, v/v) for 20 min was used to acetylate the N-terminus of MA-derived fragments, with the exception of fragment 1. Chloroactylation of the N-terminus of the R_8 peptide, was achieved with 40 equiv of chloroacetic acid, 40 equiv of diisopropylcarbodiimide and 40 equiv of 1-hydroxybenzotriazole monohydrate, treated for 1 h. Cleavage of peptides from resin and side chain deprotection were carried out by stirring for 1.5 h with a mixture of TFA, thioanisole, ethanedithiol, *m*-cresol

* Corresponding authors. Tel.: +81 3 5285 1111; fax: +81 3 5285 5037 (T.M.); tel.: +81 3 5280 8036; fax: +81 3 5280 8039 (H.M.).
E-mail addresses: tmura@nih.go.jp (T. Murakami), tamamura.mr@tmd.ac.jp (H. Tamamura).

0968-0896/$ - see front matter © 2011 Elsevier Ltd. All rights reserved.
doi:10.1016/j.bmc.2011.12.055